AUT Journal of Mechanical Engineering

AUT J. Mech. Eng., 5(3) (2021) 361-386
DOI: 10.22060/ajme.2021.18655.5911

Vibration analysis of piezoelectric graphene platelets micro-plates

F. Abbaspour, H. Arvin*

Faculty of Engineering, Shahrekord University, Shahrekord, Iran

ABSTRACT: Free and forced vibration analyses of micro-plates reinforced with graphene platelets integrated with piezoelectric layers are presented. For thermo-electrical vibration examination, a uniform temperature field and a constant external electric field along the thicknesses of the piezoelectric layers are considered. On the other hand, a uniform in-plane load is regarded along the micro-plate edges for a mechanical free vibration analysis. The Halpin–Tsai micromechanical model is used to estimate the material properties of each layer of the graphene platelets of core layer. A convergence examination is conducted to reach a functionally graded dispersion of graphene platelets layers despite the implementation of several individual graphene platelets layers. Four different distribution patterns of graphene platelets are considered to examine the vibration features for simply-supported boundary condition employing Navier's technique. Several numerical studies are accomplished to demonstrate the effects of the weight fraction, the distribution pattern, the width and the length of the graphene platelets besides the material length scale parameter, the thickness of the piezoelectric layers, the micro-plate length to the core layer thickness ratio, the applied voltage, the temperature change and the in-plane force on the natural frequencies and the time history response. The results demonstrate that in thermal environment not only reinforcing with graphene platelets does not improve the structural stiffness but also deteriorates it.

Review History:

Received: Jun. 30, 2020
Revised: Nov, 04, 2020
Accepted: Dec. 24, 2020
Available Online: Jan. 01, 2021

Keywords:

Thermo-electrical vibrations
Micro-plate
Graphene platelet
Halpin-Tsai micromechanical model
Piezoelectric layer

1- Introduction

Nowadays, micro-plates are a concern of many researchers in various scientific branches because of their widespread applications in numerous industrial fields serving as micro-resonators and micro actuators. On the other hand, the application of graphene platelets (GPLs) as a reinforcement material for improving the mechanical properties of other host structures is developed thanks to their high tensile strength and Young's modulus. Hence, investigating the vibration characteristics of isotropic micro plates as a basic element reinforced with the GPLs integrated with piezoelectric layers (piezoelectric GPL micro-plates) seems necessary.

Some available studies in the realm of free vibration of micro and macro piezoelectric plates and GPL plates are as follow. To show the novelty of the current research the presented papers are categorized into three different groups. First, a background on the researchers which have analyzed the mechanics of macro-plates with piezo-layers is presented. Next, the papers on macro-plates reinforced with GPLs are reviewed. Finally, some more related researches about micro-plates which in their formulations the size dependency is incorporated are discussed.

Many researchers have worked on the vibrations of plates with attached piezo-layers employing the classical continuum theories for plates. Askari Farsangi et al. [1] studied the free vibration of moderately thick multi-layer piezoelectric plates. The governing equations were established resorting the Mindlin theory assumptions for the plates. Levy's technique was implemented to estimate the natural frequencies. The piezoelectric layer thicknesses, as well as the plate aspect ratio influences on the natural frequencies, were examined. They indicated that the natural frequencies are impressed by the elastic stiffness elements in the closed circuit condition while the piezoelectricity exhibits its significance in the open circuit condition. Free vibration analysis of carbon nanotube (CNT) reinforced plates integrated with piezoelectric layers was examined by Kiani [2]. The governing equations were on the basis of the first order shear deformation theory for the plates. The Ritz technique was employed to extract the natural frequencies. The piezoelectric layers thicknesses, the CNT volume fraction and the CNT dispersion profile influences on the natural frequencies were studied. The outcomes demonstrated the stiffening effects of the piezoelectricity in the open circuit conditions. Bouazza and Zenkour [3] examined the linear natural frequencies of CNT reinforced composite plates employing a refined higher order theory.

Recently, the vibration analysis of GPL macro-plates is also in the spotlight of researchers. Shen et al. [4] examined

*Corresponding author's email: hadi.arvin@sku.ac.ir

the nonlinear free vibration of functionally graded (FG) GPL plates formulated on the basis of the higher order shear deformation plate theory in thermal environment. A two-step perturbation approach was employed to derive the nonlinear natural frequencies. The findings revealed a reduction treatment for the nonlinear natural frequencies owing to the increment of the temperature as well as the foundation stiffness decrement. The free and forced vibration analyses of FG GPL plates formulated based on the first order shear deformation theory were presented by Song et al. [5]. The Halpin-Tsai micromechanical model was employed to define the GPL layer effective Young's modulus while the rule of mixtures determined the effective mass density as well as the Poisson's ratio of the GPL layer. Resorting the Navier's technique the numerical results were achieved. The outcomes demonstrated that the natural frequencies and the vibration amplitude are impressed significantly by adding a small amount of GPL weight fraction. García-Macías et al. [6] presented the bending and the free vibration analyses of plates reinforced with CNTs versus the GPLs. By the implementation of the Mori-Tanaka micromechanical model the mechanical properties of the structure were obtained. Making use of the finite element (FE) approach the numerical results were extracted. The outcomes demonstrated that the GPL plates are stiffer than the CNT plates when the same amount of reinforcement weight fractions is implemented. Gholami and Ansari [7] examined the nonlinear forced vibration of GPL rectangular plates subjected to harmonic excitation. The governing equations were developed employing the third order shear deformation plate theory. The time periodic discretization was applied to the discretized equations of motion achieved by the Galerkin approach to obtain a set of nonlinear algebraic equations. This set of nonlinear algebraic equations was treated by the pseudo arc-length continuation technique beside the modified Newton-Raphson method. The results revealed that the GPL reduces the vibration amplitude and increases the natural frequencies especially in adding low-order amount of the GPL weight fraction. Qaderi et al. [8] investigated the free vibration of GPL plates in thermal environment. The equations of motion were on the basis of the higher order shear deformation theory. The Halpin-Tsai micromechanical model was employed to determine the mechanical properties of the GPL layers. The results indicated that the natural frequencies enlarge by reinforcing the matrix regardless of the GPL distribution pattern. The free vibration analysis of GPL plates was examined by Pashmforoush [9] on the basis of the Reddy third order shear deformation theory. The Halpin-Tsai micromechanical model was implemented to estimate the GPL layers mechanical properties. The FE approach was applied the governing equations to obtain the natural frequencies. He declared that the GPL weight factions, as well as the plate boundary conditions, are the two significant parameters in the determination of the GPL plate natural frequencies. Stability and the vibration of porous GPL plates with piezoelectric layers undergo supersonic flow were considered by Saidi et al. [10]. The first order shear deformation plate theory defined the displacement field relations. The Galerkin approach was applied on the governing equations to extract the numerical outcomes. The findings illustrated that the open loop natural frequencies are greater than the closed loop ones. Moreover, the stability of the GPL plate developed significantly in consequence of the increment of the GPL weight fraction.

The versatility of MEMS such as micro resonators has pushed the topics of researches to analyze the mechanics of microplates. On the other hand, sub-size plates behave differently in some aspects with respect to the macro-plates. In this respect, non-classical continuum theories have been established based on experimental and computer simulations or even continuum mechanics science to have more precise models confirming the real treatment of micro plates. Chen and Li [11] developed a new modified couple stress theory (MCST) for composite laminated Kirchhoff plates. The proposed theory considered two more length scale parameters than the ad-hoc MCST for fiber and matrix. Nonlinear bending examination of circular microplates subjected to a transverse uniform load was studied by Wang et al. [12] on the basis of a size-dependent Kirchhoff plate theory. Yue et al. [13] proposed a nonclassical Kirchhoff plate theory including the surface effects in the framework of strain gradient theory and surface elasticity theory. They inferred that the surface-induced internal residual stress impact is on the other side of the influences of the length scale parameter as well as the surface residual stress. The Kirchhoff plate theory was implemented by Li and Ma [14] to study the free vibrations of FG microplates with thermoelastic damping. They inferred that minimum thermoelastic damping can be defined by the adjustment of the physical and geometrical properties of the FG microplate. Abbaspour and Arvin [15] studied the vibrations and thermal buckling of FG micro-plates with centrosymmetric piezoelectric facesheets employing the consistent couple stress theory. They deduced that the flexoelectricity enhances the structural stiffness and consequently the natural frequency, as well as the critical thermal buckling temperature, steps up. They proposed a closed form relation which defines the natural frequencies. Arefi et al. [16] investigated the size dependent free vibration of FG micro plates integrated with piezo-magnetic layers resting on the Pasternak foundation. The MCST alongside the first order shear deformation plate theory was implemented to derive the governing equations. The Navier's approach was applied on the equations of motion to achieve the natural frequencies. The findings revealed an ascending trend for the natural frequencies by the growth of the core layer thickness to the piezoelectric layers thickness ratio due to its stiffening impact on the structural flexural rigidity.

Considering the literature review, we can see that the mechanics of MEMS reinforced with GPLs have not been examined yet. On the other hand, these micro-structures are usually coupled with piezo-layers in order to be capable for mass sensing purposes and also in various micro-actuators. Accordingly, a study on the free and forced vibration attributes of micro plates reinforced with graphene platelets with piezoelectric layers (piezoelectric GPL micro plates) is

required to find out the significant impression of the GPLs reinforcements in thermo-electrical loading conditions of such structures usually employed in MEMS. Hence, this paper deals with the mechanical free vibration and the thermo-electrical free and forced vibration investigations of piezoelectric GPL micro plates. The Halpin–Tsai micromechanical model is employed for the determination of the effective mechanical properties of the GPL layers. The governing equations are developed based on the Kirchhoff plate theory assumptions in accompany with the MCST to enrich the equations of motion with the size effects. The Navier's technique is utilized to derive the free and forced vibration aspects of simply-supported piezoelectric GPL micro plates. A comparison of the current outcomes with the available results in the literature reveals the validity of the current formulation and the findings. A convergence study is accomplished to achieve a continuous variation of the GPL layers mechanical properties along the micro plate core layer thickness, i.e. FG distribution of GPLs, even with making use of few GPL layers. The effects of the temperature difference, the external voltage, the in-plane load, the GPL distribution pattern, the GPL weight fraction, the GPL layer length, the GPL layer width, the piezoelectric layers thicknesses to the host layer thickness ratio, the micro plate length to the host layer thickness proportion and the host layer thickness to the material length scale parameter ratio on the fundamental natural frequency and the time history response are investigated.

2- Mathematical Modeling

2- 1- Fundamental relations

In order to enrich the governing equations with the size effects, the MCST is employed. Accordingly, the strain energy for a structure occupying volume $\forall$, including the electrical effects, can be expressed by [2, 17]:

$$U = \frac{1}{2}\int_{\forall}\left(\sigma_{ij}\varepsilon_{ij} + m_{ij}\chi_{ij} - D_i E_i\right)d\forall \tag{1}$$

where σ_{ij}, ε_{ij}, m_{ij}, χ_{ij}, D_i and E_i represent the stress tensor, the strain tensor, the deviatoric part of the symmetric couple stress tensor, the symmetric curvature tensor, the electric displacement vector and the electric field vector, respectively.

The deviatoric part of the symmetric couple stress tensor is defined by [17]:

$$m_{ij} = 2\mu l^2 \chi_{ij} \tag{2}$$

in which l and μ indicate the length scale parameter and the shear modulus, respectively. The symmetric curvature tensor is determined through [17]:

$$\chi_{ij} = \frac{1}{2}\left(\theta_{i,j} + \theta_{j,i}\right) \tag{3}$$

where θ_i is the rotation vector described by [17]:

$$\theta_i = \frac{1}{2}e_{ijk}u_{k,j} \tag{4}$$

in which u_k and e_{ijk} denote the displacement field vector and the permutation tensor, respectively.

The stress tensor components for the plane stress condition are determined by [18]:

$$\begin{Bmatrix}\sigma_{xx}\\ \sigma_{yy}\\ \sigma_{xy}\end{Bmatrix} = \begin{bmatrix}Q_{11} & Q_{12} & 0\\ Q_{21} & Q_{22} & 0\\ 0 & 0 & Q_{66}\end{bmatrix}\begin{Bmatrix}\varepsilon_{xx}\\ \varepsilon_{yy}\\ \gamma_{xy}\end{Bmatrix} - \begin{bmatrix}0 & 0 & e_{31}\\ 0 & 0 & e_{32}\\ 0 & 0 & 0\end{bmatrix}\begin{Bmatrix}E_x\\ E_y\\ E_z\end{Bmatrix} - \begin{bmatrix}Q_{11} & Q_{12} & 0\\ Q_{21} & Q_{22} & 0\\ 0 & 0 & 0\end{bmatrix}\begin{Bmatrix}\alpha_{11}\Delta T\\ \alpha_{22}\Delta T\\ 0\end{Bmatrix} \tag{5}$$

in which e_{31} and e_{32} point out the piezoelectric constants and Q_{ij}'s represent the effective orthotropic elastic coefficients for the plane stress condition presented in Eq. (A.5) in **Appendix**. Moreover, ΔT is the temperature change and α_{11} and α_{22} stand for the thermal expansion coefficients.

The strain tensor is defined through the Green-Lagrange strain displacement relation [18]:

$$\varepsilon_{ij} = \frac{1}{2}\left[u_{i,j} + u_{j,i} + u_{k,i}u_{k,j}\right] \tag{6}$$

Furthermore, the electric displacement vector components are described by [18]:

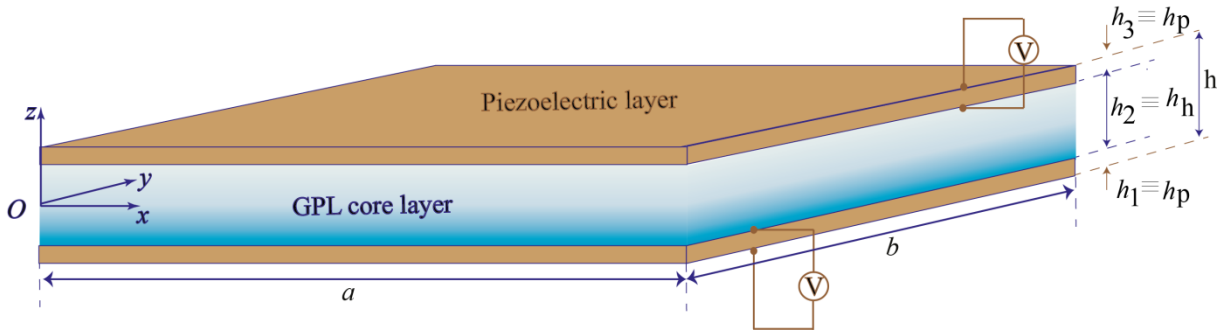

Fig. 1. Geometry of an FG GPL (A-Pattern) micro plate integrated with piezoelectric layers.

$$\begin{Bmatrix} D_x \\ D_y \\ D_z \end{Bmatrix} = \begin{bmatrix} 0 & 0 & 0 \\ 0 & 0 & 0 \\ e_{31} & e_{32} & 0 \end{bmatrix} \begin{Bmatrix} \varepsilon_{xx} \\ \varepsilon_{yy} \\ \gamma_{xy} \end{Bmatrix} + \begin{bmatrix} k_{11} & 0 & 0 \\ 0 & k_{22} & 0 \\ 0 & 0 & k_{33} \end{bmatrix} \begin{Bmatrix} E_x \\ E_y \\ E_z \end{Bmatrix} + \begin{bmatrix} p_1 & 0 & 0 \\ 0 & p_2 & 0 \\ 0 & 0 & p_3 \end{bmatrix} \Delta T \tag{7}$$

in which p_i 's and k_{ii} 's are the pyroelectric coefficients and the dielectric permittivity constants, respectively.

2- 2- The micro plate geometry

The geometrical view of a three-layered simply-supported rectangular micro plate undergoes external voltages, *V,* is depicted in Fig. 1. *a*, *b* and *h*, are, respectively the length, the side and the total thickness of the micro plate. The *x*- and the *y*- axes are oriented along the micro plate length and width, respectively, while the *z*-axis is directed along the micro plate thickness. The origin of the (*x*,*y*,*z*) coordinate system, i.e. *O*, is located at the left corner of the micro plate mid-plane. The host layer is made of epoxy reinforced with FG GPLs. The bottom and the top surfaces of the host layer are integrated with two piezoelectric layers with thicknesses equal to h_1 and h_3, respectively.

The electric field vector is determined by [2]:

$$E_i = -\varphi_{,i} \tag{8}$$

in which φ is the electric potential. It is assumed that, the bottom and the top piezoelectric layers are subjected to external voltages, V . According to [19], the spatial form of the electric potential division for each piezoelectric layer can be considered as (Eq. (6a) in [19]):

$$\varphi_1(x,y,z) = \phi_1(z)\psi_1(x,y) + Vf_1(z) \tag{9}$$

$$\varphi_3(x,y,z) = \phi_3(z)\psi_3(x,y) + Vf_3(z) \tag{10}$$

in which $\psi_1(x,y)$ and $\psi_3(x,y)$ are, respectively, the in-plane dispersion of the bottom and the top piezoelectric layers electric potentials while $\phi_i(z)$ and $f_i(z)$ denote, respectively, the distribution of the electric potential and the external voltage along with the piezoelectric layer thicknesses. Consistent with Eq. (6a) in [19] the electric potential may be considered as a combination of a half-cosine and a linearly varying term to satisfy Maxwell's equation. The half-cosine term must vanish at the bottom and top surfaces of the piezolayer and becomes minus one at the mid-plane of the piezolayer. On the other side, the linear term must vanish at the mid-plane of the piezolayers and becomes one and minus one, respectively, at the top and bottom surfaces of the piezolayers. In this respect, the distribution of the electric potential and the external voltage along the bottom and the top piezoelectric layers thicknesses can be considered as

$$\phi_1(z) = -\cos\left(\pi\left(\frac{2z + h_2 + h_1}{2h_1}\right)\right),$$

$$\phi_3(z) = -\cos\left(\pi\left(\frac{2z - h_2 - h_3}{2h_3}\right)\right),$$

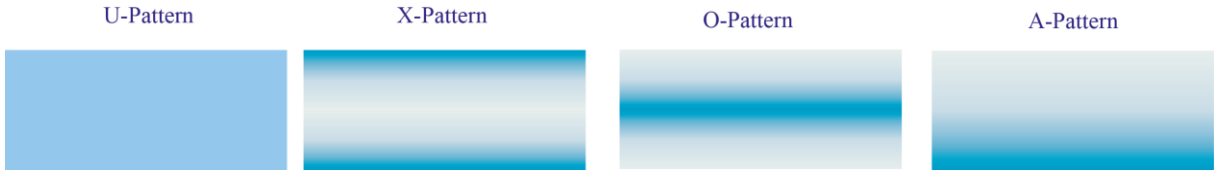

Fig. 2. FG GPL distribution patterns.

$$f_1(z)=\frac{2z+h_2}{2h_1} \text{ and } f_3(z)=\frac{2z-h_2}{2h_3}.$$

2- 3- The effective mechanical properties of a GPL layer

Four considered different FG GPL distribution patterns are depicted in Fig. 2.

Due to manufacturing matters, it is hard to access an FG GPL distribution pattern. Hence, a number of GPL layers with different GPL volume fraction are assembled to reach something like continuous mechanical properties. A convergence examination which is presented in *Sect*. 4.2.1 reveals how many layers are required to have this continuity. The *k*th layer volume fraction, i.e. $V_{GPL}^{(k)}$, for different distribution patterns is prescribed by [20, 21] as:

$$U-Pattern: V_{GPL}^{(k)}=V_{GPL}^{*} \tag{11}$$

$$X-Pattern: V_{GPL}^{(k)}=2V_{GPL}^{*}\left|2k-N_L-1\right|/N_L \tag{12}$$

$$O-Pattern: V_{GPL}^{(k)}=2V_{GPL}^{*}\left(1-\left|2k-N_L-1\right|/N_L\right) \tag{13}$$

$$A-Pattern: V_{GPL}^{(k)}=V_{GPL}^{*}\left(\left|2k-1\right|/N_L\right) \tag{14}$$

where N_L is the total number of the GPL layers of the host layer and V_{GPL}^{*} is the total GPLs volume fraction in the host layer assigned by [20]:

$$V_{GPL}^{*}=\frac{W_{GPL}}{W_{GPL}+\left(\frac{\rho^{GPL}}{\rho^{m}}\right)\left(1-W_{GPL}\right)} \tag{15}$$

in which W_{GPL}, ρ^{GPL} and ρ^{m} stand, respectively, for the GPL weight fraction and the GPL and the matrix mass densities.

Employing the rule of mixture, the GPL layers Poisson's ratio and the thermal expansion coefficient can be presented, respectively, by [20]:

$$\nu=V_{GPL}^{*}\nu^{GPL}+V_m\nu^{m} \tag{16}$$

$$\alpha=V_{GPL}\alpha^{GPL}+V_m\alpha^{m} \tag{17}$$

in which ν^{GPL} and ν^{m} are, respectively, the GPL and the matrix Poisson's ratios and α^{GPL} and α^{m} are, respectively, the GPL and the matrix thermal expansion coefficients. Furthermore, V_m indicates the matrix volume fraction which is related to the GPL layer volume fraction, i.e. V_{GPL}, as follows [20]:

$$V_{GPL}+V_m=1 \tag{18}$$

According to the Halpin-Tsai micromechanical model, the GPL layer effective Young's modulus read as [20]:

$$E=\frac{3}{8}\frac{1+\xi_L\eta_L V_{GPL}}{1-\eta_L V_{GPL}}E_m+\frac{5}{8}\frac{1+\xi_T\eta_T V_{GPL}}{1-\eta_T V_{GPL}}E_m \tag{19}$$

in which E_m is the matrix Young's modulus and the other parameters are defined by [20]:

$$\xi_L = 2\frac{a_{GPL}}{t_{GPL}}, \xi_T = 2\frac{b_{GPL}}{t_{GPL}} \tag{20}$$

$$\eta_L = \frac{E_{GPL}/E_m - 1}{E_{GPL}/E_m + \xi_L}, \quad \eta_T = \frac{E_{GPL}/E_m - 1}{E_{GPL}/E_m + \xi_T} \tag{21}$$

where E_{GPL} is the GPL Young's modulus and a_{GPL}, b_{GPL} and t_{GPL} are the GPL length, width and thickness, respectively.

2- 4- Deriving the governing equations

According to the assumptions of the Kirchhoff plate theory, the displacement field components can be expressed by [18]:

$$u_1 = u_0(x,y) - z\frac{\partial w(x,y)}{\partial x}$$
$$u_2 = v_0(x,y) - z\frac{\partial w(x,y)}{\partial y} \tag{22}$$
$$u_3 = w(x,y)$$

where u_0 and v_0 are, respectively, the in-plane displacements of the core mid-plane along the *x* and *y* axes while w is the transverse deflection of the core mid-plane.

The substitution of Eq. (22) into Eq. (6) in accompany with the von-Karman strain-displacement assumptions [18], delivers the non-zeros strain components:

$$\varepsilon_{xx} = \left[\varepsilon_{xx}^0\right] + z\left\{\varepsilon_{xx}^1\right\} \equiv \left[\frac{\partial u_0}{\partial x} + \frac{1}{2}\left(\frac{\partial w}{\partial x}\right)^2\right] + z\left\{-\frac{\partial^2 w}{\partial x^2}\right\}$$
$$\varepsilon_{yy} = \left[\varepsilon_{yy}^0\right] + z\left\{\varepsilon_{yy}^1\right\} \equiv \left[\frac{\partial v_0}{\partial y} + \frac{1}{2}\left(\frac{\partial w}{\partial y}\right)^2\right] + z\left\{-\frac{\partial^2 w}{\partial y^2}\right\} \tag{23}$$
$$\varepsilon_{xy} = \left[\varepsilon_{xy}^0\right] + z\left\{\varepsilon_{xy}^1\right\} \equiv \left[\frac{1}{2}\left(\frac{\partial u_0}{\partial y} + \frac{\partial v_0}{\partial x}\right) + \frac{1}{2}\frac{\partial w}{\partial x}\frac{\partial w}{\partial y}\right] + z\left\{-\frac{\partial^2 w}{\partial x\,\partial y}\right\}$$

where ε_{ij}^0 and ε_{ij}^1 ($i, j = x$ and y), denote, respectively, the membrane and the flexural strains.

The substitution of Eq. (22), into Eq. (4) reveals the rotation vector components:

$$\theta_x = \frac{\partial w}{\partial y}, \quad \theta_y = -\frac{\partial w}{\partial x}, \quad \theta_z = \frac{1}{2}\left(\frac{\partial v_0}{\partial x} - \frac{\partial u_0}{\partial y}\right) \tag{24}$$

Thereafter, the deviatoric part of the symmetric couple stress tensor is achieved making use of Eqs. (2), (3) and (24).

Accordingly, the consideration of the non-zero strain and the symmetric curvature tensor components develops the strain energy, Eq. (1), to:

$$U = \frac{1}{2}\int_{\forall}(\sigma_{xx}\varepsilon_{xx} + \sigma_{yy}\varepsilon_{yy} + 2\sigma_{xy}\varepsilon_{xy} + m_{xx}\chi_{xx} + m_{yy}\chi_{yy} + 2m_{xy}\chi_{xy} + 2m_{yz}\chi_{yz} + 2m_{xz}\chi_{xz})d\forall + \frac{1}{2}\int_{\forall}(-D_{1x}E_{1x} - D_{1y}E_{1y} - D_{1z}E_{1z} - D_{3x}E_{3x} - D_{3y}E_{3y} - D_{3z}E_{3z})d\forall \tag{25}$$

Eventually, the strain energy for the piezoelectric GPL micro plate is released by the substitution of Eqs. (5), (7), (23) and the resulting nonzero components of the deviatoric part of the symmetric couple stress tensor into Eq. (25).

On the other hand, the kinetic energy in keeping with $T = \frac{1}{2}\int_{\forall}\rho_i \dot{u}_i^2 d\forall$ [22] in which ρ_i is the mass density of the *i*th layer, read as:

$$T = \frac{1}{2}\int_0^b\int_0^a\left(I_0\dot{u}_0^2 + I_0\dot{v}_0^2 + I_2\left(\left(\frac{\partial \dot{w}}{\partial x}\right)^2 + \right. \right. \tag{26}$$

$$\left(\frac{\partial \dot{w}}{\partial y}\right)^2\Bigg)+I_0\dot{w}^2-2I_1\left(\dot{u}_0\frac{\partial \dot{w}}{\partial x}+\dot{v}_0\frac{\partial \dot{w}}{\partial y}\right)\Bigg)dxdy$$

where I_j 's stand for the micro plate inertial coefficients defined by:

$$I_j=\int_{z_1}^{z_2}\rho_1 z^j dz+\int_{z_2}^{z_3}\rho_2 z^j dz+\int_{z_3}^{z_4}\rho_3 z^j dz\ \left(j=0,1\text{and}2\right) \tag{27}$$

in which $z_1=-\frac{h_2}{2}-h_1$, $z_2=-\frac{h_2}{2}$, $z_3=\frac{h_2}{2}$, and $z_4=\frac{h_2}{2}+h_3$.

Resorting the Hamilton's principle [22], i.e. $\int_{t_1}^{t_2}(\delta T-\delta U)dt=0$, the nonlinear governing equations of motion are derived:

$$\begin{aligned}&\frac{\partial^2 M_{xx}}{\partial x^2}+\frac{\partial^2 M_{yy}}{\partial y^2}+2\frac{\partial^2 M_{xy}}{\partial x\,\partial y}+\\&N_{xx}\frac{\partial^2 w}{\partial x^2}+N_{yy}\frac{\partial^2 w}{\partial y^2}+2N_{xy}\frac{\partial^2 w}{\partial x\,\partial y}-\\&\frac{\partial^2 Y_{xx}}{\partial x\,\partial y}+\frac{\partial^2 Y_{yy}}{\partial x\,\partial y}-\frac{\partial^2 Y_{xy}}{\partial y^2}+\frac{\partial^2 Y_{xy}}{\partial x^2}=\\&I_0\ddot{w}-I_2\left(\frac{\partial^2 \ddot{w}}{\partial x^2}+\frac{\partial^2 \ddot{w}}{\partial y^2}\right)+I_1\left(\frac{\partial \ddot{u}_0}{\partial x}+\frac{\partial \ddot{v}_0}{\partial y}\right)\end{aligned} \tag{28}$$

$$\begin{aligned}&\frac{\partial N_{xx}}{\partial x}+\frac{\partial N_{xy}}{\partial y}+\frac{1}{2}\frac{\partial^2 Y_{zy}}{\partial y^2}+\\&\frac{1}{2}\frac{\partial^2 Y_{zx}}{\partial x\,\partial y}=I_0\ddot{u}_0-I_1\left(\frac{\partial \ddot{w}}{\partial x}\right)\end{aligned} \tag{29}$$

$$\begin{aligned}&\frac{\partial N_{yy}}{\partial y}+\frac{\partial N_{xy}}{\partial x}-\frac{1}{2}\frac{\partial^2 Y_{zy}}{\partial x\,\partial y}-\\&\frac{1}{2}\frac{\partial^2 Y_{zx}}{\partial x^2}=I_0\ddot{v}_0-I_1\left(\frac{\partial \ddot{w}}{\partial y}\right)\end{aligned} \tag{30}$$

$$\begin{aligned}&\int_{z_3}^{z_4}\left(\begin{array}{l}-\phi_3^2\left(k_{11}^{(3)}\frac{\partial^2\psi_3}{\partial x^2}+k_{22}^{(3)}\frac{\partial^2\psi_3}{\partial y^2}\right)+\\k_{33}^{(3)}\phi_{3,z}\left(\phi_{3,z}\psi_3+Vf_3'(z)\right)-p_3^{(3)}\phi_{3,z}\Delta T\end{array}\right)dz\\&-\frac{1}{2}\left(E_{31}^{(3)}\left(\frac{\partial w}{\partial x}\right)^2+E_{32}^{(3)}\left(\frac{\partial w}{\partial y}\right)^2\right)-\\&\left(E_{31}^{(3)}\frac{\partial u_0}{\partial x}+E_{32}^{(3)}\frac{\partial v_0}{\partial y}\right)+\\&\left(H_{31}^{(3)}\frac{\partial^2 w}{\partial x^2}+H_{32}^{(3)}\frac{\partial^2 w}{\partial y^2}\right)=0\end{aligned} \tag{31}$$

$$\begin{aligned}&\int_{z_1}^{z_2}\left(\begin{array}{l}-\phi_1^2\left(k_{11}^{(1)}\frac{\partial^2\psi_1}{\partial x^2}+k_{22}^{(1)}\frac{\partial^2\psi_1}{\partial y^2}\right)+\\k_{33}^{(1)}\phi_{1,z}\left(\phi_{1,z}\psi_1+Vf_1'(z)\right)-p_3^{(1)}\phi_{1,z}\Delta T\end{array}\right)dz\\&-\frac{1}{2}\left(E_{31}^{(1)}\left(\frac{\partial w}{\partial x}\right)^2+E_{32}^{(1)}\left(\frac{\partial w}{\partial y}\right)^2\right)-\\&\left(E_{31}^{(1)}\frac{\partial u_0}{\partial x}+E_{32}^{(1)}\frac{\partial v_0}{\partial y}\right)+\\&\left(H_{31}^{(1)}\frac{\partial^2 w}{\partial x^2}+H_{32}^{(1)}\frac{\partial^2 w}{\partial y^2}\right)=0\end{aligned} \tag{32}$$

where M_{ij}, N_{ij} and Y_{ij} are the moment and the axial force resultants and the higher-order moment resultants defined, respectively, in Eqs. (A.2), (A.1) and (A.7) in **Appendix**. In addition, $E_{3i}^{(j)}$ and $H_{3i}^{(j)}$ are related the piezoelectric constants and the distribution of the electric potential along the piezoelectric layer thicknesses determined by:

$$\left(E_{3i}^{(j)},H_{3i}^{(j)}\right)=\int_{z_3}^{z_4}e_{3i}^{(j)}\left(1,z\right)\phi_{j,z}dz,\quad i=1,2\text{and}\,j=1,3 \tag{33}$$

For the sake of brevity, the associated boundary conditions and also the displacement form of the governing partial differential equations are presented, respectively, in Eqs. (A.15)-(A.34) and (A.10)-(A.14) in **Appendix**.

3- Solution strategy

To extract the free and forced vibration analysis outcomes for an immovable simply-supported piezoelectric FG GPL micro plate, the Navier's solution is employed. In this respect, according to the considered type of boundary supports for the

micro plate, some essential and natural conditions must be satisfied. The essential conditions for the displacement field components and the in-plane electric potential may be written as:

$$\begin{aligned} &@x=0,a: u_0=w=\psi_1=\psi_3=0 \\ &@y=0,b: v_0=w=\psi_1=\psi_3=0 \end{aligned} \tag{34}$$

while for the sake of brevity the natural boundary conditions are presented in Eqs. (A.15)-(A.34) in Appendix. For satisfying the mentioned boundary conditions and the natural boundary conditions reported in **Appendix** the displacement field components and the in-plane electric potential distributions are regarded, respectively, as:

$$u_0(x,y,t)=\sum_n\sum_m U_{mn}(t)N_u(x,y) \tag{35}$$

$$v_0(x,y,t)=\sum_n\sum_m V_{mn}(t)N_v(x,y) \tag{36}$$

$$w(x,y,t)=\sum_n\sum_m W_{mn}(t)N_w(x,y) \tag{37}$$

$$\psi_1(x,y,t)=\sum_n\sum_m P_{1mn}(t)N_\psi(x,y) \tag{38}$$

$$\psi_3(x,y,t)=\sum_n\sum_m P_{3mn}(t)N_\psi(x,y) \tag{39}$$

where $N_u(x,y)=\sin\left(\frac{m\pi x}{a}\right)\cos\left(\frac{n\pi y}{b}\right)$,

$N_v(x,y)=\cos\left(\frac{m\pi x}{a}\right)\sin\left(\frac{n\pi y}{b}\right)$,

$N_w(x,y)=\sin\left(\frac{m\pi x}{a}\right)\sin\left(\frac{n\pi y}{b}\right)$,

and $N_\psi(x,y)=\sin\left(\frac{m\pi x}{a}\right)\sin\left(\frac{n\pi y}{b}\right)$ and U_{mn}, V_{mn}, W_{mn}, P_{1mn} and P_{3mn} are the time dependent amplitude of the in-plane and transverse displacements and the time dependent amplitude of the in-plane electric potential dispersions, respectively. Moreover, *m* and *n* are related to the natural frequency mode number. It should be pointed out that in the case of the immovable boundary conditions the mechanical in-plane load is considered zero and only the symmetric GPL distribution patterns are examined.

3- 1- Free vibration analysis

In the case of the thermo-electrical free vibration analysis a harmonic variation for the displacement and the electrical amplitudes are considered such as $\mathbf{u}(t)=\bar{\mathbf{u}}\sin(\omega t)$ and $\psi(t)=\bar{\psi}\sin(\omega t)$ in which $\bar{\mathbf{u}}=\left[\bar{U}_{mn},\bar{V}_{mn},\bar{W}_{mn}\right]^{\mathrm{T}}$, $\bar{\psi}=\left[\bar{P}_{1mn},\bar{P}_{3mn}\right]^{\mathrm{T}}$ and ω is the corresponding natural frequency. Considering the aforementioned harmonic variations for the displacement and the electrical amplitudes, Eqs. (35)-(39) are substituted into the left hand side of the linearized version of the governing equations, Eqs. (A.10)-(A.14). The weighted residual technique [22] is applied on the ensuing relations. Accordingly, a proper weighting function is multiplied to each ensuing relation and the resultant is integrated on the domain of the micro-plate. In this regard, respectively, $N_u(x,y)$, $N_v(x,y)$, $N_w(x,y)$, $N_\psi(x,y)$ and $N_\psi(x,y)$ are the appropriate weighting functions for these five resulting relations. For example, for Eq. (A.10) we have:

$$\int_0^a\int_0^b N_u(x,y)\left[\begin{pmatrix}\text{ensuing relation by the substitution of}\\ \text{Eqs.(35) to (39) into the linearized version}\\ \text{of the left hand side of Eq.(A.10)}\end{pmatrix}\right]\mathrm{d}y\mathrm{d}x=0$$

Consequently, a set of equations which delivers the natural frequencies is deduced:

$$-\omega^2\begin{bmatrix}\mathbf{M}_{uu} & 0\\ 0 & 0\end{bmatrix}\begin{pmatrix}\bar{\mathbf{u}}\\ \bar{\boldsymbol{\psi}}\end{pmatrix}+\begin{bmatrix}\mathbf{K}_{uu} & \mathbf{K}_{u\psi}\\ \mathbf{K}_{\psi u} & \mathbf{K}_{\psi\psi}\end{bmatrix}\begin{pmatrix}\bar{\mathbf{u}}\\ \bar{\boldsymbol{\psi}}\end{pmatrix}=\begin{pmatrix}0\\ 0\end{pmatrix} \tag{40}$$

in which M_{uu} is the mass matrix, K_{uu} is the elastic matrix, $\mathbf{K}_{u\psi}$ is the piezoelectric matrix, $\mathbf{K}_{\psi u}=\mathbf{K}_{u\psi}{}^{\mathrm{T}}$ and $\mathbf{K}_{\psi\psi}$ is the permittivity matrix.

In this paper, two different electrical boundary conditions are examined; the open and the closed circuit electrical conditions. In the open circuit condition, the electric potential amplitude vector is obtained from the second row of Eq. (40) as $\bar{\psi}=-\mathbf{K}_{\psi\psi}{}^{-1}\times\mathbf{K}_{\psi u}\bar{\mathbf{u}}$. Replacing the resulting electric potential vector into the first row of Eq. (40) delivers a standard eigen-value problem which releases the natural frequencies for the open circuit condition:

$$\left(\mathbf{K}_{uu}-\mathbf{K}_{u\psi}\mathbf{K}_{\psi\psi}{}^{-1}\mathbf{K}_{\psi u}\right)\bar{\mathbf{u}}=\boldsymbol{\omega}^2\mathbf{M}_{uu}\bar{\mathbf{u}} \tag{41}$$

On the other hand, for the closed circuit condition in

which the piezoelectric layers surfaces are short-circuited, the electric potential amplitude vector is $\bar{\psi}=0$ and subsequently, from Eq. (40), the eigen-value problem which leads to the natural frequencies for the closed circuit conditions read as:

$$\mathbf{K}_{uu}\bar{\mathbf{u}}=\omega^2\mathbf{M}_{uu}\bar{\mathbf{u}} \tag{42}$$

For the evaluation of the free vibration features in terms of the external in-plane load the movable boundary conditions are adjusted and all four GPL dispersion patterns are analyzed. Meanwhile, the temperature change and the external applied voltage are considered zero. In this case, the in-plane axial displacement read as:

$$u_0(x,y,t)=\sum_n\sum_m U_{mn}(t)\cos\left(\frac{m\pi x}{a}\right)\sin\left(\frac{n\pi y}{b}\right) \tag{43}$$

$$v_0(x,y,t)=\sum_n\sum_m V_{mn}(t)\sin\left(\frac{m\pi x}{a}\right)\cos\left(\frac{n\pi y}{b}\right) \tag{44}$$

Moreover, the following adjustment for a uniform compressive in-plane force is required to apply on Eq. (28), $N_{xx}=N_{yy}\equiv -N_0$ and $N_{xy}=0$. The same route which was expressed for the thermo-electrical free vibration examination leads to the closed and the open circuit conditions natural frequencies.

3- 2- Forced vibration analysis

A distributed external transverse force is considered as $F(x,y,t)=F(t)\sin\left(\frac{m\pi x}{a}\right)\sin\left(\frac{n\pi y}{b}\right)$ to analyze the forced vibration aspects. In this condition, the micro plate is motivated to vibrate in its (m,n) *th* mode shape configuration. Subsequently, the implementation of the Navier's technique results in:

$$\begin{bmatrix}\mathbf{M}_{uu} & 0\\ 0 & 0\end{bmatrix}\begin{pmatrix}\ddot{\mathbf{u}}(t)\\ \ddot{\boldsymbol{\psi}}(t)\end{pmatrix}+\begin{bmatrix}\mathbf{K}_{uu} & \mathbf{K}_{u\psi}\\ \mathbf{K}_{\psi u} & \mathbf{K}_{\psi\psi}\end{bmatrix}\begin{pmatrix}\mathbf{u}(t)\\ \boldsymbol{\psi}(t)\end{pmatrix}=\begin{pmatrix}\mathbf{F}\\ 0\end{pmatrix} \tag{45}$$

in which $\mathbf{F}=\left[0\quad 0\quad \int_0^a\int_0^b F(x,y,t)\sin\left(\frac{m\pi x}{a}\right)\sin\left(\frac{n\pi y}{b}\right)\mathrm{d}y\mathrm{d}x\right]^{\mathrm{T}}$.

Eq. (45) consists of 5 ordinary differential equations (ODEs) although a similar procedure as *Sect. 3.1.* reduces this set of ODEs to 3 coupled ODEs for both the closed and the open circuit conditions. Assuming zero initial conditions, the forced vibration response can be determined through the methodology released in *Sect. 4.10* of [22].

4- Results and Discussion

4- 1- Verification

In order to validate the free vibration results, a square simply-supported FG GPL plate with piezoelectric layers formulated based on the Reddy third order shear deformation plate theory assumptions is considered [23]. The polygonal FE formulation method has been implemented in [23] to extract the natural frequencies. The core layer is made of Copper as the matrix phase which is reinforced by the GPLs. The number of the GPL layers is $N_L=10$. Moreover, the Young's modulus, the mass density and the Poisson's ratio of the Copper are, respectively, 130 (GPa), 8960 ($\mathrm{kg/m^3}$) and 0.34 [23]. Furthermore, the Young's modulus, the mass density and the Poisson's ratio coefficient of the GPL are, respectively, 1010 (GPa), 1062.5 ($\mathrm{kg/m^3}$) and 0.186 [23]. The piezoelectric layers are made of PZT-4 with the following electro-mechanical properties:

$E_{11}=E_{22}=81.3(\mathrm{GPa}), \nu_{12}=0.33, G_{12}=\frac{E_{11}}{2(1+\nu_{12})}=30.6(\mathrm{GPa})$, $\rho=7600$ ($\mathrm{kg/m^3}$), $d_{31}=d_{32}=-1.22\times10^{-10}$ (m/Volt), $k_{11}=k_{22}=1475\,\varepsilon_0$ (F/m), $k_{33}=1300\,\varepsilon_0$ (F/m) and $\varepsilon_0=8.85\times10^{-12}$ (F/m) [23]. The plate geometrical data are a=b=1 (m), h_2=50 (mm), $h_1=h_3=1$ (mm), a_{GPL}=2.5 $(\mu\mathrm{m})$, b_{GPL} =1.5 $(\mu\mathrm{m})$ and t_{GPL} =1.5 (nm). The first natural frequency for the closed circuit condition and for the two cases of the GPL weight fraction, 0.5 % and 1 % are presented in Table 1. A difference percent below 1 indicates a good agreement. Hence the outcomes illustrate the authority of the current results in GPL reinforcing modeling.

The second validating study is the assessment of the current formulation in preserving the size dependency. The sample is a square simply-supported single layer micro plate modeled based on the Kirchhoff plate theory alongside the MCST [24]. The Levy's solution has been implemented in [24] to extract the natural frequencies. The plate is made of Epoxy with Young's modulus, the mass density and the Poisson's ratio, respectively, equal to 1.44 (GPa), 1220 ($\mathrm{kg/m^3}$) and 0.38. The geometrical data and the material length scale parameter are, respectively, a=b=10 (mm) and l=17.6. μm The first natural frequency for two cases of the micro plate thickness, i.e. h=l and h=10l, on the basis of the classical continuum theory (l=0) and the MCST assumptions are presented in Table 2. It should be pointed out that the results from [24] are extracted from Fig. 6 of the above-mentioned reference. Excellent conformity is achieved.

4- 2- Parametric studies and discussions

After the authentication of the current outcomes, some case studies for a simply-supported piezoelectric FG GPL micro plate are carried out in this section. The host layer is made of several Epoxy layers reinforced with different GPL weight

Table 1. The current first natural frequency for a square simply-supported piezoelectric FG GPL plate versus the corresponding value reported in [23] (Hz).

U-Pattern	Present results	212.807	235.532
	Results of [23]	211.560	234.182
	Difference %	0.59	0.58
X-Pattern	Present results	228.148	262.329
	Results of [23]	226.503	260.176
	Difference %	0.73	0.83
A-Pattern	Present results	212.916	232.258
	Results of [23]	211.677	231.014
	Difference %	0.58	0.54

Table 2. The present first natural frequency for a square micro plate versus the corresponding value reported in [24] (rad/s).

		Classical theory results (*l*=0)		**MCST results**	
		Current	[24]	Current	[24]
$h/l=1$		1177.9	1176.2	2559.1	2560.4
	Difference %	0.14		0.05	
$h/l=10$		11776.2	11776.2	11993.3	11995.4
	Difference %	0.00		0.02	

fractions. Both of the piezoelectric layers on the bottom and the top of the host layer are made of PZT-5A. The Young's modulus, the mass density, the Poisson's ratio and the thermal expansion coefficient of the Epoxy are, respectively, 3 (GPa), 1200 ($\mathrm{kg/m^3}$), 0.34 and 60 ($\times 10^{-6}$/K) [20]. Furthermore, the Young's modulus, the mass density, the Poisson's ratio and the thermal expansion coefficient of the GPL are, respectively, 1010 (GPa), 1062.5 ($\mathrm{kg/m^3}$), 0.186 and 5×10^{-6}/K [20]. In addition, the GPL geometrical data and weight fraction are, respectively, a_{GPL}=2.5 μm , b_{GPL}=1.5 μm and t_{GPL}=1.5 (nm) and $W_{GPL}=0.3\%$ [20]. The shear modulus for the host layer is $Q_{66}=\frac{E}{2(1+\nu)}$ [20]. Moreover, the Young's modulus, the shear modulus, the mass density, the Poisson's ratio and the thermal expansion coefficient for the PZT-5A are, respectively, 63 (GPa), 24.2 (GPa), 7600 ($\mathrm{kg/m^3}$), 0.35, 0.9 ($\times 10^{-6}$/K) and the piezoelectric coefficients are $e_{31}=e_{32}=$ -7.209 $(\mathrm{C/m^2})$, $e_{24}=e_{15}=12.322$ $(\mathrm{C/m^2})$, $k_{11}=k_{22}=1.53\times10^{-8}$ $(\mathrm{W/m^{\circ}K})$, $k_{33}=1.5\times10^{-8}$ $(\mathrm{W/m^{\circ}K})$ [25]. On the other hand, the geometrical features for the micro plate are: $a/b=1$, $b/h_h=25$, $h_p=\frac{h_h}{8}$ and $h_h/l=1$ in which *l*=17.6 μm . Furthermore, the temperature change, ΔT , is set to zero. Henceforth, the preceding geometrical attributes, thermal loading condition and the MCST as a base theory are assumed for the current extracted outcomes for the FG GPL micro plate unless new values or theories are prescribed in specific investigations.

4- 2- 1- Convergence analysis

At first, to have an accurate FG GPL model with continuity in the mechanical properties as well as the vibration treatment instead of a multi-layered GPL layers with discontinuity in the aforementioned features, a convergence analysis is established here. Hereafter, the presented findings are for the open circuit condition when $V\neq0$ and for the closed circuit condition

Table 3. The first natural frequency (Mrad/s) for a square piezoelectric multi-layered GPL micro plate on the basis of the MCST for different dispersion patterns and external voltages versus the number of the GPL layers incorporated in the assemblage of the core layer.

	Circuit condition	Open			Closed		
		U	X	O	U	X	**O**
$N_L=2$	$V=-50$ Volt	4.043	4.043	4.043			
	$V=0$ Volt	3.874	3.874	3.874	3.874	3.874	**3.874**
	$V=50$ Volt	3.698	3.698	3.698			
$N_L=4$	$V=-50$ Volt	4.043	4.057	4.029			
	$V=0$ Volt	3.874	3.888	3.860	3.874	3.888	**3.860**
	$V=50$ Volt	3.698	3.712	3.683			
$N_L=6$	$V=-50$ Volt	4.043	4.059	4.028			
	$V=0$ Volt	3.874	3.891	3.858	3.874	3.891	**3.858**
	$V=50$ Volt	3.698	3.715	3.680			
$N_L=8$	$V=-50$ Volt	4.043	4.060	4.026			
	$V=0$ Volt	3.874	3.892	3.856	3.874	3.892	**3.856**
	$V=50$ Volt	3.698	3.716	3.679			
$N_L=10$	$V=-50$ Volt	4.043	4.061	4.026			
	$V=0$ Volt	3.874	3.892	3.856	3.874	3.892	**3.856**
	$V=50$ Volt	**3.698**	**3.717**	**3.679**			

when $V=0$. The first natural frequency on the basis of the MCST for different numbers of GPL layers included in the core layer is presented in Table 3 and graphically in Fig. 3. It is found that for $N_L=10$ the convergence is occurred for both the open and the closed circuit conditions. Consequently, in the future all the outcomes for the piezoelectric FG GPL micro plate are calculated and depicted for $N_L=10$.

4- 2- 2- Free vibration analysis

Micro plate geometrical characteristics analysis In this section, the variation of the fundamental natural frequency with respect to the micro plate geometrical features is assessed.

The variation of the first natural frequency on the basis of the MCST and the classical theory (CT) ($l=0$) in terms of the piezoelectric layers thicknesses to the host layer thickness ratio, i.e. h_p/h_h, is demonstrated in Fig. 4 for different GPL distribution patterns when V=50 (Volt). It should be noted that the host layer thickness has been kept constant and only the thickness of the piezoelectric layers increases identically. It is perceived that by the increase of the h_p/h_h ratio, the fundamental natural frequency increases. This trend is due to the stiffening of the structure which is followed by the enhancement of the piezoelectric layer thicknesses. The other implication is that always the X-, U-, A- and O-Patterns, have, respectively, the maximum to the minimum natural frequency owing to the specific intensity division of various FG GPLs. Moreover, the FG GPL distribution pattern impact on the natural frequency is more distinctive for the lower magnitudes of the h_p/h_h ratio especially when there is no piezoelectric layers attached to the host layer. Although the distinction between the FG GPL patterns is more apparent for the CT results, Furthermore, the MCST predicts higher natural frequency.

The first natural frequency versus the core layer thickness to the material length scale parameter ratio, i.e. h_h/l, is shown in Fig. 5. It can be seen that by the growth of the h_h/l ratio, the natural frequency declines as a result of the stiffening influence of the material length scale parameter on the structure. Moreover, the first natural frequency is more impressed by the FG GPL dispersion pattern with the augmentation of the h_h/l ratio.

The changeability of the first natural frequency in terms of the micro plate length to the core layer thickness ratio, i.e. a/h_h, is depicted in Fig. 6 based on the CT and the MCST. A descending trend for the natural frequency is observed since the increment of the a/h_h ratio, makes the structure thinner and subsequently reduces the structural stiffness.

GPL attributes analysis After the assessment of the micro plate geometrical characteristics impacts on the first

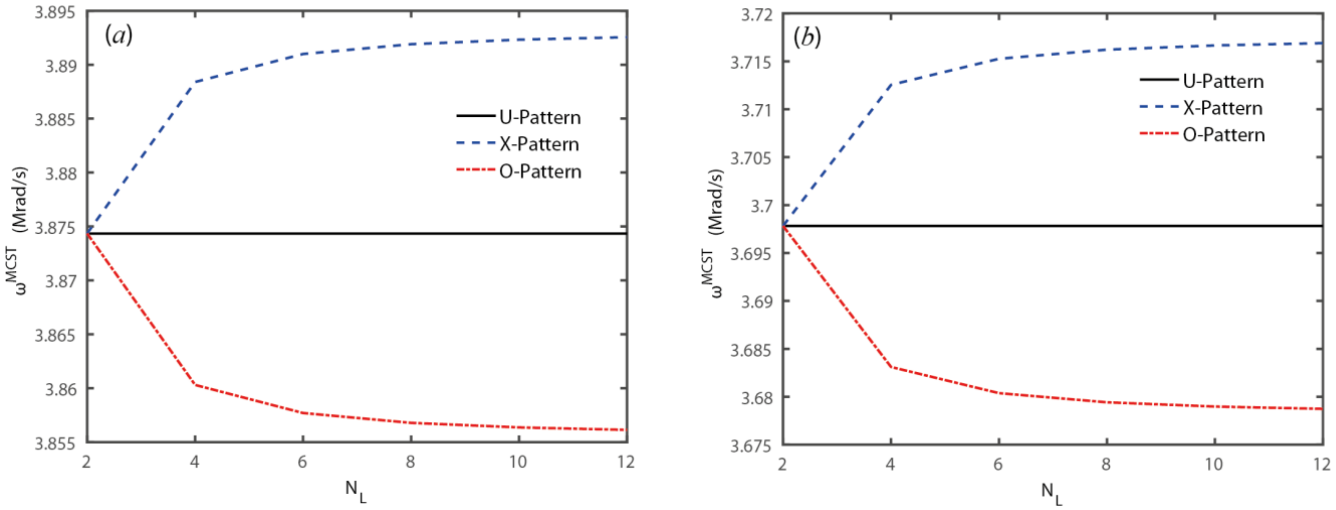

Fig. 3. The first natural frequency (Mrad/s) for a square piezoelectric multi-layered GPL micro plate on the basis of the MCST for different dispersion patterns versus the number of the GPL layers incorporated in the assemblage of the core layer (a)-V= 0 (Volt) and (b)- V= 50 (Volt).

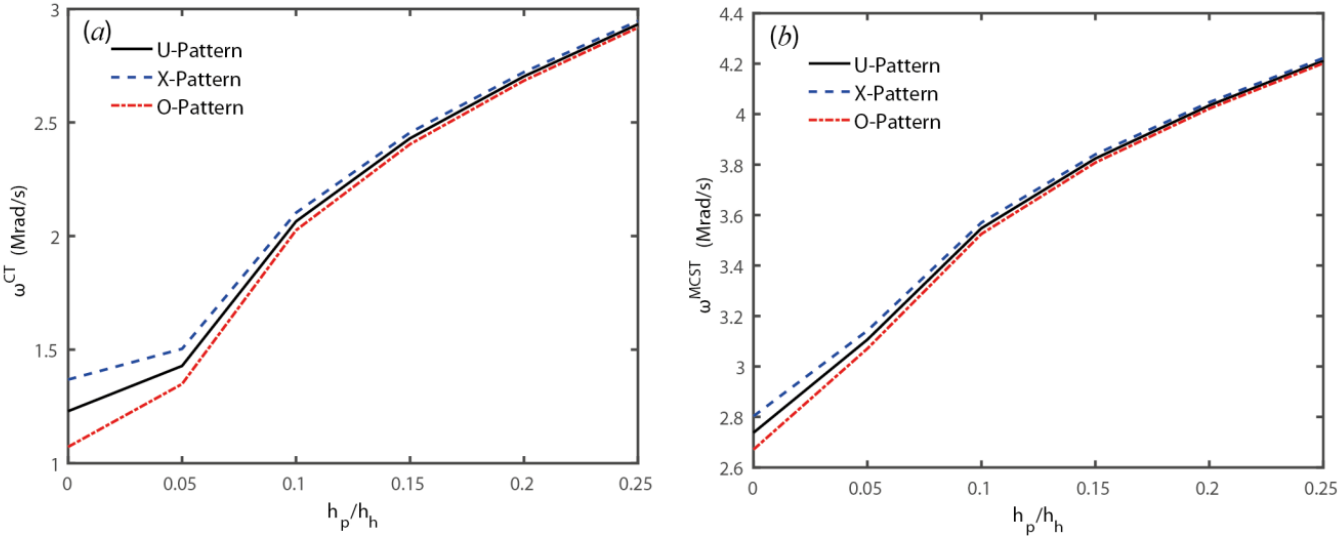

Fig. 4. The first natural frequency (Mrad/s) for a square piezoelectric multi-layered GPL micro plate in terms of the piezoelectric layers thicknesses to the host layer thickness ratio, h_p / h_h , based on the (a)-CT and the (b)-MCST (V=50 (Volt)).

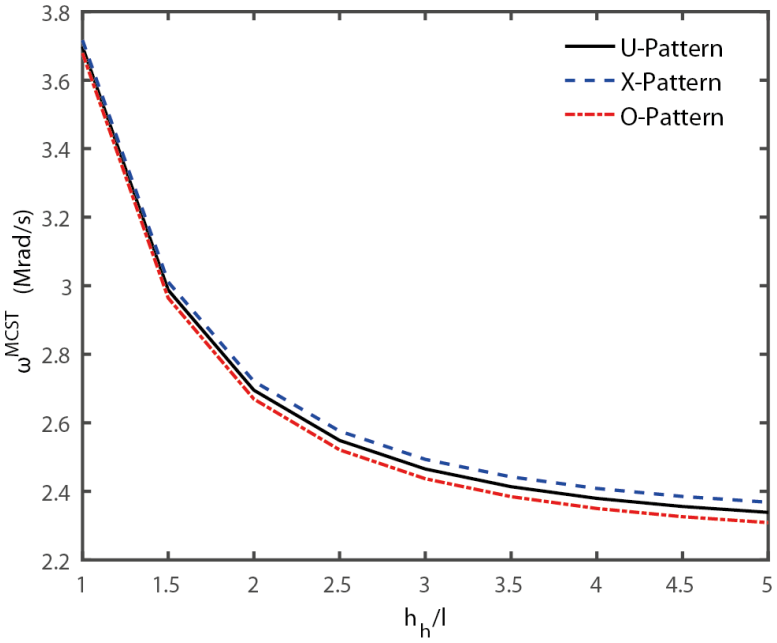

Fig. 5. The first natural frequency (Mrad/s) for a square piezoelectric FG GPL micro plate in terms of the host layer thickness to the material length scale parameter ratio, h_h / l , based on the MCST, (V=50 (Volt)).

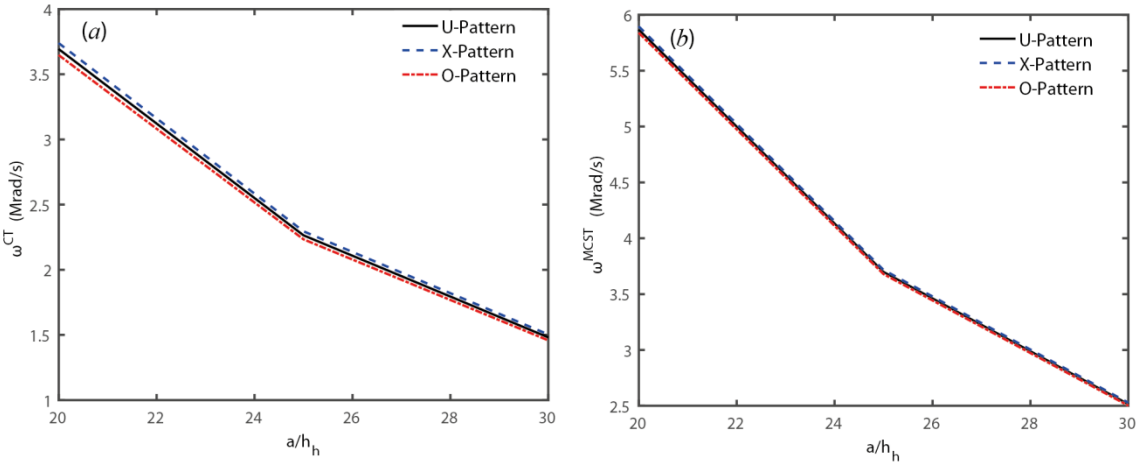

Fig. 6. The first natural frequency (Mrad/s) for a square piezoelectric FG GPL micro plate in terms of the micro plate length to the host layer thickness ratio, a / h_h , based on the (a)-CT and the (b)-MCST, (V=50 (Volt)).

natural frequency, the GPL geometrical aspects as well as the GPL weight fraction effects on the fundamental natural frequency for three different external voltages, i.e. V= -50, 0 and 50 (Volt), are examined in this section.

The influence of the GPL side, b_{GPL} , on the first natural frequency is demonstrated in Fig. 7. It can be observed that the increment of b_{GPL} is accompanied with the ascendant of the natural frequency. On the other hand, by the growth of b_{GPL} the FG GPL dispersion pattern impact is boosted. Moreover, by the enhancement of the external voltage, the natural frequency reduces thanks to the resulting electric compressive force which makes the structure weaker. It is worth to note that, according to Eq. (A.1) presented in **Appendix**, the sign of the resulting electric force is negative (positive) as a consequence of positive (negative)

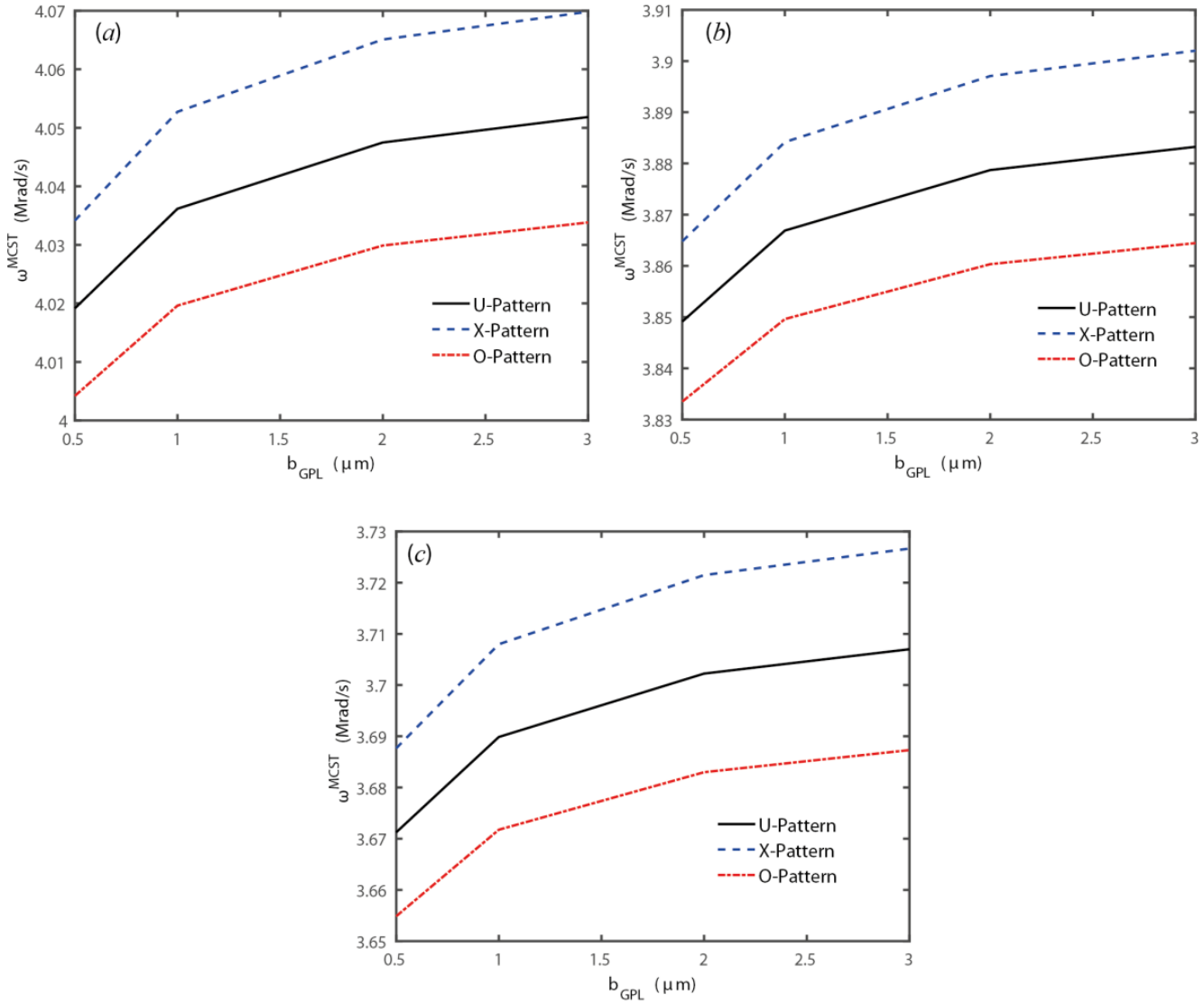

Fig. 7. The first natural frequency (Mrad/s) for a square piezoelectric FG GPL micro plate in terms of the GPL side, b_{GPL} , based on the MCST (a)- V=-50 (Volt), (b)- V=0 (Volt) and (c)- V=50 (Volt).

voltages and the sign of e_{31} and e_{32} which are negative here. Subsequently, a positive (negative) voltage generates a compressive (tensile) axial force.

The variation of the fundamental natural frequency versus a_{GPL} is shown in Fig. 8. The figure indicates an ascending trend for the first natural frequency by the augmentation of a_{GPL} . Moreover, although by the increment of a_{GPL} the GPL distribution pattern impact on the natural frequency is more noticeable however this feature is not comparable with b_{GPL} variation influence.

The fundamental natural frequency versus the GPL weight fraction, W_{GPL} , is depicted in Fig. 9. As a result of the GPL weight fraction augmentation the natural frequency increases. Furthermore, the significance of the GPL dispersion pattern is manifested with the growth of the GPL weight fraction.

Thermo-electrical free vibration analysis In this section the simultaneous interaction of the temperature change and the external voltage on the fundamental natural frequency is examined in Fig. 10. The Fig. predicts a descending treatment for the natural frequency as a result of the temperature augmentation. Consequently, at a threshold value of the temperature change depends on the external voltage magnitude the fundamental natural frequency degenerates.

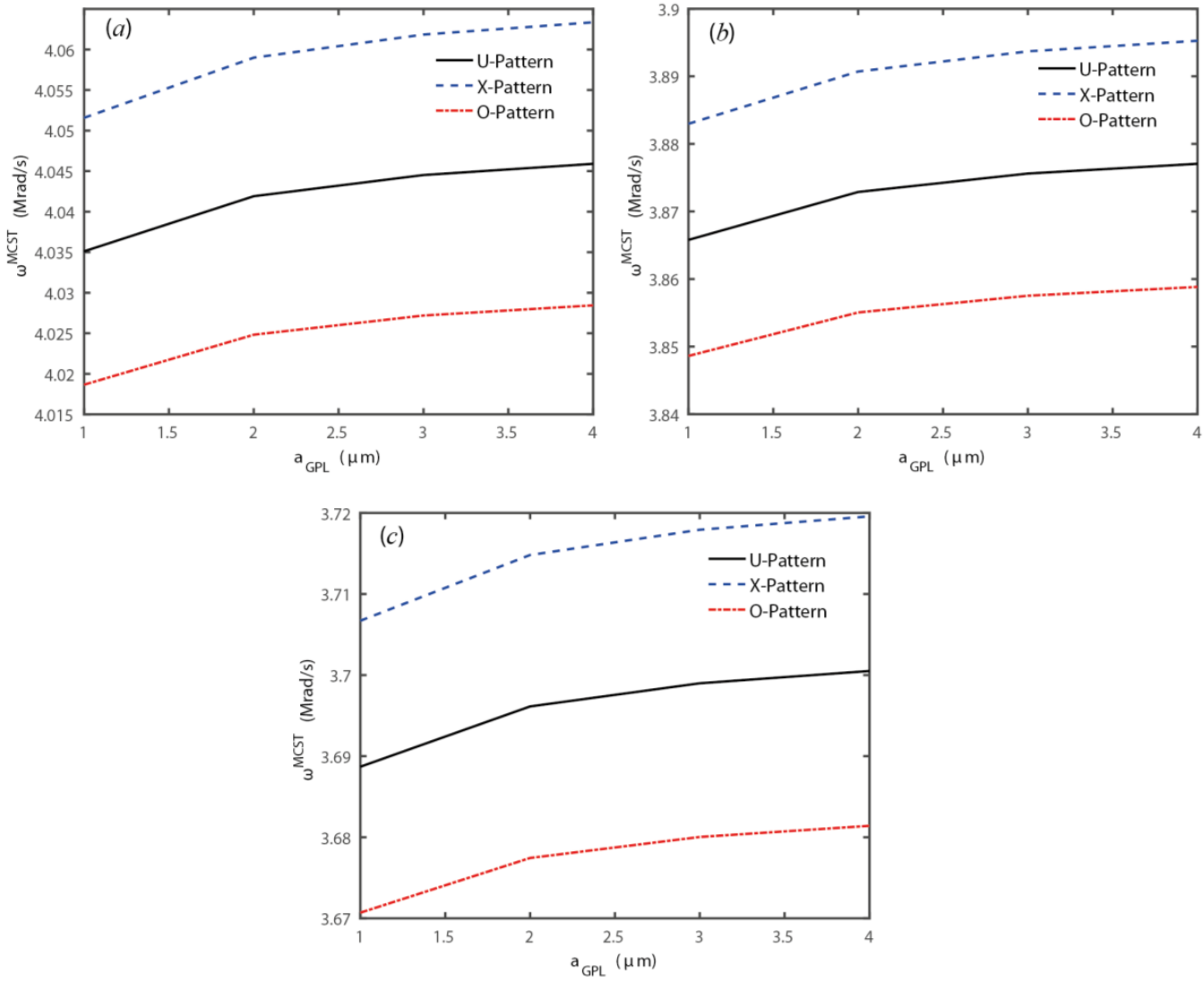

Fig. 8. The first natural frequency (Mrad/s) for a square piezoelectric FG GPL micro plate versus the GPL length, a_{GPL} , based on the MCST (a)- V=-50 (Volt), (b)- V=0 (Volt) and (c)- V=50 (Volt).

This phenomenon is directly associated with the thermo-electrical buckling of the FG GPL micro plate. Although, the aforementioned threshold value for the temperature change can be postponed by a negative external voltage.

For more illustration the voltage influence on the fundamental natural frequency of an FG-X GPL micro plate for two different magnitudes of the temperature change is shown in Fig. 11. The figure indicates that the natural frequency reduces by the augmentation of the external voltage due to the similar reason explained in the opening of *Sect. 4.2.2*.

Mechanical free vibration analysis The effect of the nondimensional uniform compressive in-plane load, $\hat{N}_0 = \frac{N_0 a^2}{E_m h^3}$, on the fundamental natural frequency is examined in Fig. 12. As afore mentioned in *Sect. 3*. the present outcomes are for a movable simply-supported micro plate and the temperature change and the external voltage are equal to zero. As expected the natural frequency decreases as a consequence of stepping up the nondimensional in-plane load from a tensile in-plane load (at left) to a compressive load (at right) which consequently yields to the buckling of the micro plate. The nondimensional critical buckling load, $\hat{N}_0$, for the U-, X-, O- and A-Patterns, respectively, is determined

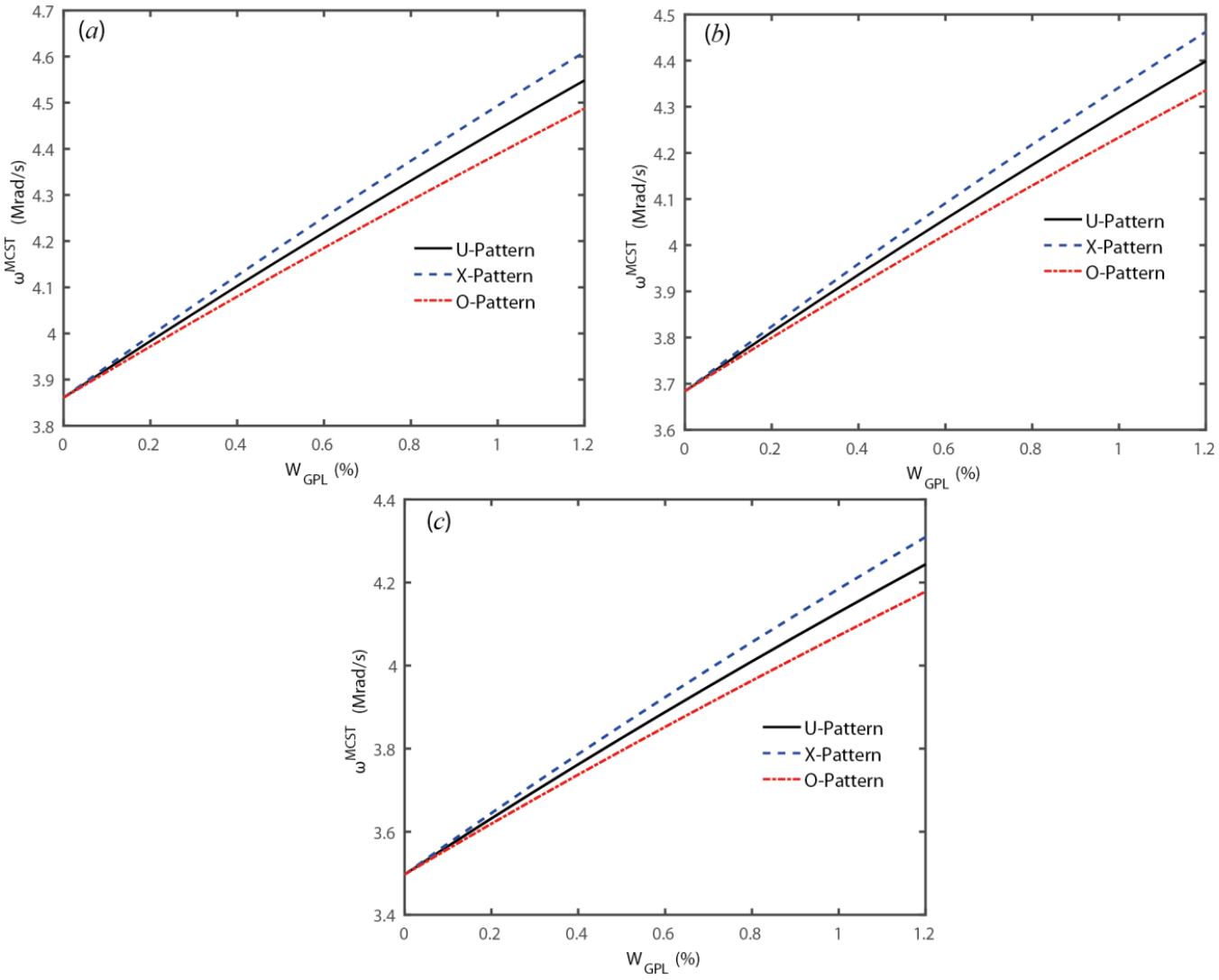

Fig. 9. The first natural frequency (Mrad/s) for a square piezoelectric FG GPL micro plate versus the GPL weight fraction, W_{GPL} , based on the MCST (a)- V=-50, (Volt), (b)- V=0 (Volt) and (c)- V=50 (Volt).

equal to 95.748, 96.638, 94.861, 95.665.

4- 2- 3- Thermo-electrical forced vibration analysis

The forced vibration analysis is addressed here. The external transverse force distribution is assumed as $F(x,y,t)=F_0u(t)\sin\frac{\pi x}{a}\sin\frac{\pi y}{b}$ to directly excite the first mode in which $u(t)$ is the step function. The nondimensional amplitude of the external force is taken as $\hat{F}_0=5$ where $\hat{F}_0=\frac{F_0a^2}{E_mh_h^3}$. The time history response of the micro plate center $^m(x,y)=(a/2,b/2)$ for an immovable piezoelectric GPL simply-supported micro plate in terms of the nondimensional time $\tau=\frac{1}{a}\sqrt{(E_m/\rho_m)}t$ for a not-reinforced micro plate, $W_{GPL}=0$, and for GPL weight fraction equal to $W_{GPL}=0.3\%$ is depicted in Fig. 13. The presented results are calculated for a U GPL distribution pattern. It can be seen that when the temperature change is zero and the external voltage is zero or not the reinforced micro plate is stiffer and subsequently the micro plate deflection as well as the time period of the response is slightly smaller or in other words the fundamental natural frequency is larger in consistent with Fig. 9. Moreover, a positive external voltage always weakens

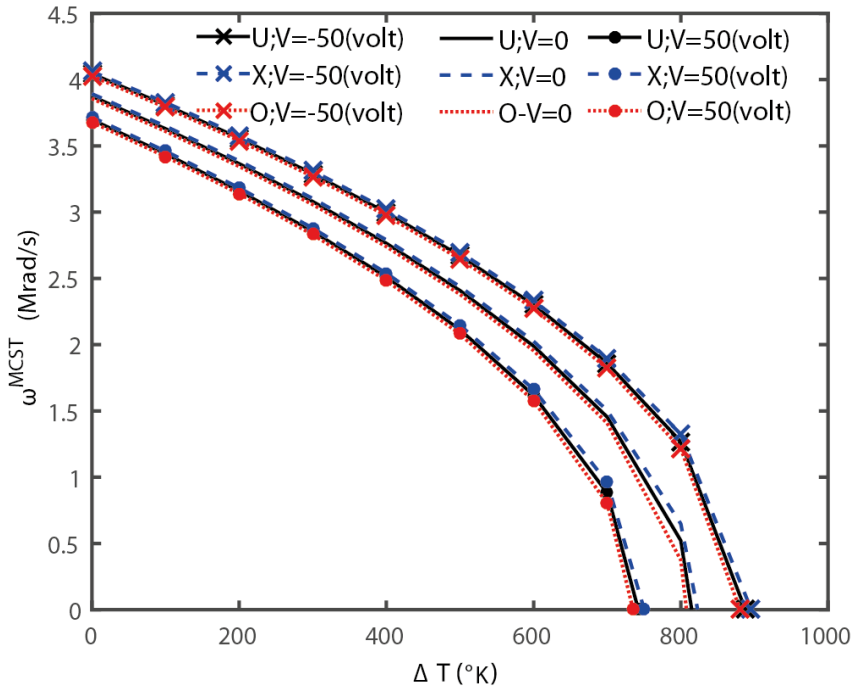

Fig. 10. The first natural frequency (Mrad/s) for a square piezoelectric FG GPL micro plate versus the temperature difference, ΔT , based on the MCST (a)- V=-50 (Volt), (b)- V=0 (Volt) and (c)- V=50 (Volt).

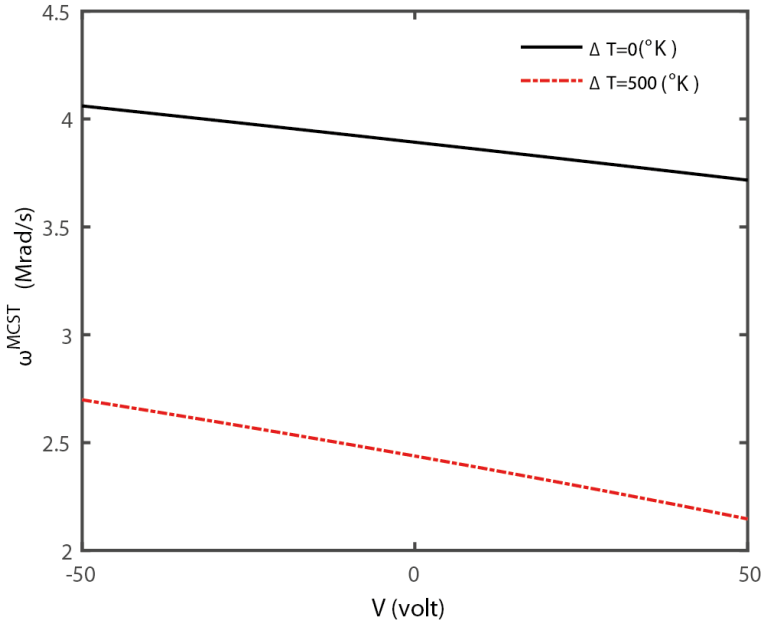

Fig. 11. The first natural frequency (Mrad/s) for a square piezoelectric FG-X GPL micro plate versus the external voltage, V, based on the MCST.

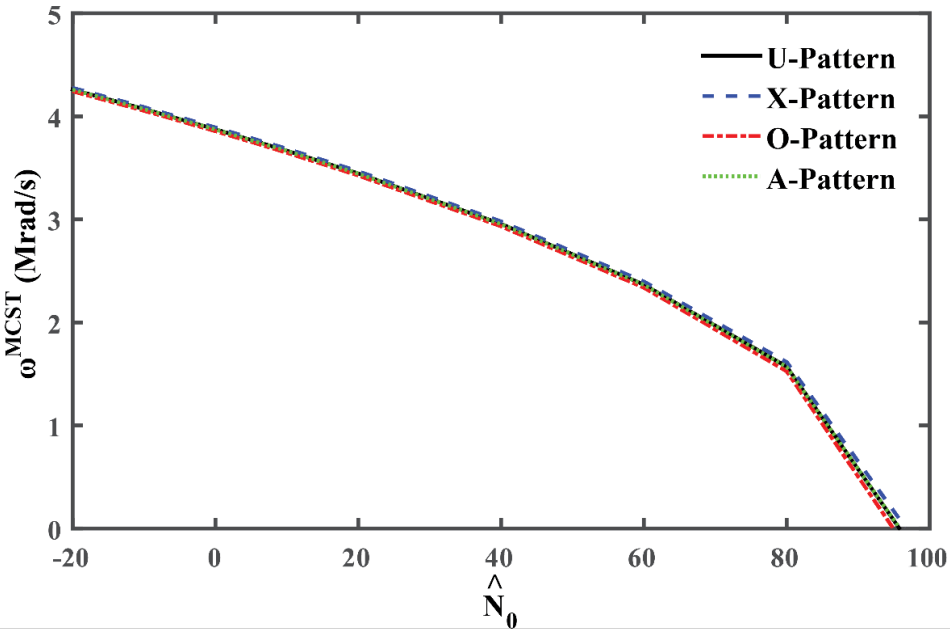

Fig. 12. The first natural frequency (Mrad/s) for a square piezoelectric FG GPL micro plate versus the uniform in-plane mechanical load based on the MCST.

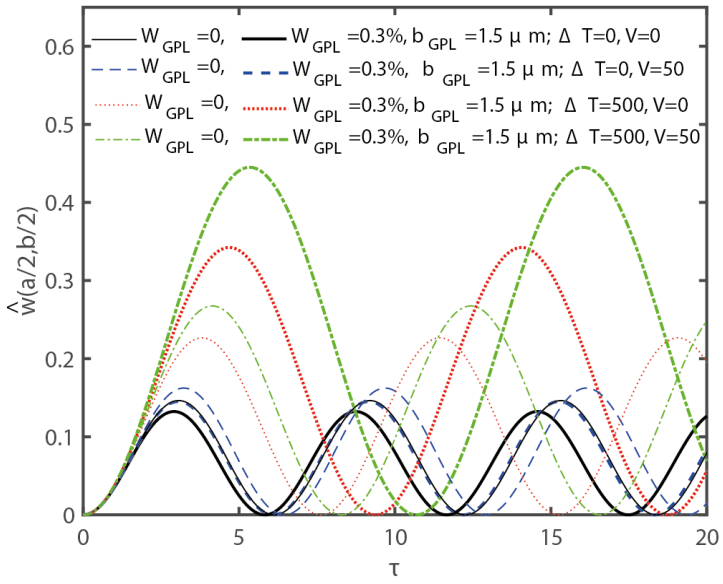

Fig. 13. The time history response of the micro plate center $(x, y) = (a/2, b/2)$ for a square immovable simply-supported piezoelectric U-GPL micro plate in terms of the nondimensional time based on the MCST ($W_{GPL} = 0$: thin lines; $W_{GPL} = 0.3\%$: thick lines).

reinforced or not-reinforced structures approximately in the same way. On the other hand, when the temperature emerges the story is different because of its contribution to induce a compressive axial force which inclines to decline the structural stiffness in contrast with the GPL weight fraction tendency. The GPL weight fraction enhancement improves to some extent the flexural rigidity comparing with the axial rigidity. Alternatively according to Eq. (A.6) the growth of the latter mutually boosts up the thermal resultant axial force when the micro plate is reinforced with the GPLs and consequently, in the thermal environment the GPL reinforcing decays the structural stiffness.

The GPL side, b_{GPL} , impact on the time history response of the micro plate center is examined in Fig. 14. The same implication as the previous study can be made. Although the GPL side augmentation stiffens the structure however the

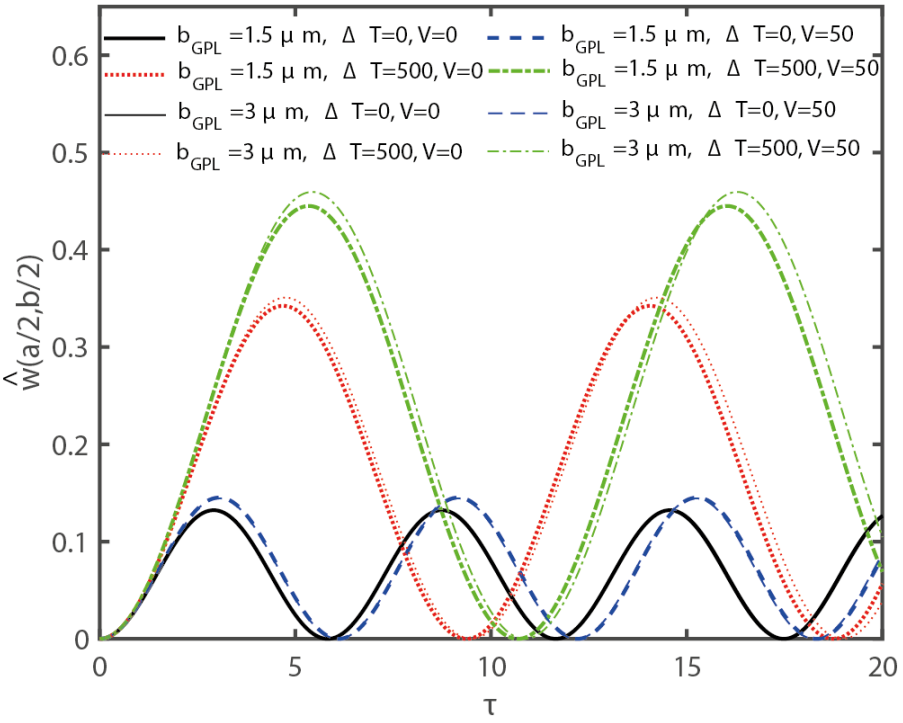

Fig. 14. The time history response of the micro plate center $(x, y) = (a/2, b/2)$ for a square immovable simply-supported piezoelectric U-GPL micro plate in terms of the nondimensional time based on the MCST ($b_{GPL} = 1.5\,\mu m$: thick lines; $b_{GPL} = 3\,\mu m$: thin lines).

stiffening is smaller than the decline caused by the thermal resultant axial force which is manifested by the GPL side enlargement. Subsequently, the micro plate deflection and the time period of the response are getting greater.

For more illustration, the two preceding time history response analyses are collected in Fig. 15. In each division of the figure the same external voltage, as well as the thermal loading, is considered. The outcomes lead to the same inference.

5- Conclusions

The mechanical free vibration and the thermo-electrical free and forced vibrations of simply-supported piezoelectric functionally graded graphene platelets micro plates were examined. The modified couple stress theory alongside the Kirchhoff plate theory assumptions were employed to derive the governing equations by the implementation of the Hamilton's principle. Resorting the Navier's approach the free and forced vibration outcomes for the closed and the open circuit conditions were extracted. The findings demonstrate:

A positive voltage as well as temperature increment declines the structural stiffness and consequently the fundamental natural frequency decreases and the deflection amplitude and the time period of the forced vibration response increases.

For immovable boundary conditions stepping up the temperature leads to the degeneration of the fundamental natural frequency which is directly interrelated with the destabilization of the micro plate due to the buckling occurrence. Although the destabilization can be postponed to higher temperature by a negative voltage.

Enlarging the GPL attributes may not always lead to boosting up the structural stiffness and it depends also on the thermal loading condition.

Enlarging the GPL attributes such as the GPL side, the GPL length and the GPL weight fraction improves the structural stiffness which subsequently results in a larger fundamental natural frequency in the absence of thermal loading.

The increment of the GPL features decays the structural stiffness when the micro plate is in thermal environment.

The GPL dispersion pattern contribution develops considerably by the reduction of the piezoelectric thickness and the material length scale parameter as well as the augmentation of the GPL weight fraction and the GPL side.

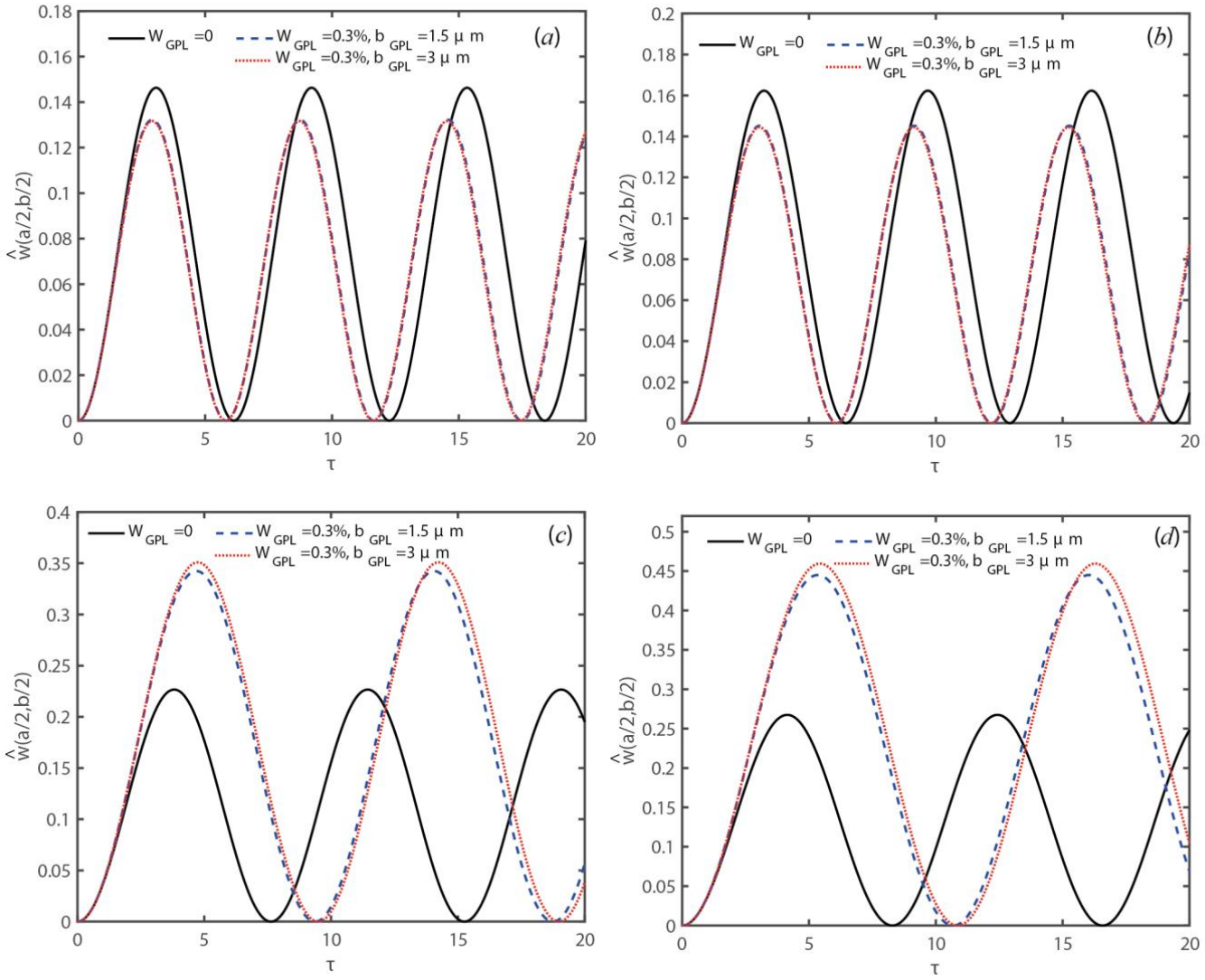

Fig. 15. The time history response of the micro plate center $(x, y) = (a/2, b/2)$ for a square immovable simply-supported piezoelectric U-GPL micro plate in terms of the nondimensional time based on the MCST, based on the MCST (a)- $\Delta T = 0$ and V=0 (Volt), (b)- $\Delta T = 0$ and V=50 (Volt), (c)- $\Delta T = 500$ K and V=0 (Volt) and (d)- $\Delta T = 500$ K and V=50 (Volt).

Appendix

The force and the moment resultants:

$$\begin{Bmatrix} N_{xx} \\ N_{yy} \\ N_{xy} \end{Bmatrix} = \sum_{k=1}^{3} \int_{z_k}^{z_{k+1}} \begin{Bmatrix} \sigma_{xx}^{(k)} \\ \sigma_{yy}^{(k)} \\ \sigma_{xy}^{(k)} \end{Bmatrix} dz = \begin{bmatrix} A_{11} & A_{12} & 0 \\ A_{12} & A_{22} & 0 \\ 0 & 0 & A_{66} \end{bmatrix} \begin{Bmatrix} \varepsilon_{xx}^{0} \\ \varepsilon_{yy}^{0} \\ \varepsilon_{xy}^{0} \end{Bmatrix} + \begin{bmatrix} B_{11} & B_{12} & 0 \\ B_{12} & B_{22} & 0 \\ 0 & 0 & B_{66} \end{bmatrix} \begin{Bmatrix} \varepsilon_{xx}^{1} \\ \varepsilon_{yy}^{1} \\ \varepsilon_{xy}^{1} \end{Bmatrix}$$
$$+ \begin{Bmatrix} \hat{E}_{31}^{(1)} + \hat{E}_{31}^{(3)} \\ \hat{E}_{32}^{(1)} + \hat{E}_{32}^{(3)} \\ 0 \end{Bmatrix} V + \begin{Bmatrix} E_{31}^{(1)} \psi_1 + E_{31}^{(3)} \psi_3 \\ E_{32}^{(1)} \psi_1 + E_{32}^{(3)} \psi_3 \\ 0 \end{Bmatrix} - \begin{Bmatrix} N_{xx}^{T} \\ N_{yy}^{T} \\ 0 \end{Bmatrix} \tag{A.1}$$

$$\begin{Bmatrix} M_{xx} \\ M_{yy} \\ M_{xy} \end{Bmatrix} = \sum_{k=1}^{3} \int_{z_k}^{z_{k+1}} \begin{Bmatrix} \sigma_{xx}^{(k)} \\ \sigma_{yy}^{(k)} \\ \sigma_{xy}^{(k)} \end{Bmatrix} z dz = \begin{bmatrix} B_{11} & B_{12} & 0 \\ B_{12} & B_{22} & 0 \\ 0 & 0 & B_{66} \end{bmatrix} \begin{Bmatrix} \varepsilon_{xx}^{0} \\ \varepsilon_{yy}^{0} \\ \varepsilon_{xy}^{0} \end{Bmatrix} + \begin{bmatrix} D_{11} & D_{12} & 0 \\ D_{12} & D_{22} & 0 \\ 0 & 0 & D_{66} \end{bmatrix} \begin{Bmatrix} \varepsilon_{xx}^{1} \\ \varepsilon_{yy}^{1} \\ \varepsilon_{xy}^{1} \end{Bmatrix}$$
$$+ \begin{Bmatrix} \hat{H}_{31}^{(1)} + \hat{H}_{31}^{(3)} \\ \hat{H}_{32}^{(1)} + \hat{H}_{32}^{(3)} \\ 0 \end{Bmatrix} V + \begin{Bmatrix} H_{31}^{(1)} \psi_1 + H_{31}^{(3)} \psi_3 \\ H_{32}^{(1)} \psi_1 + H_{32}^{(3)} \psi_3 \\ 0 \end{Bmatrix} - \begin{Bmatrix} M_{xx}^{T} \\ M_{yy}^{T} \\ 0 \end{Bmatrix} \tag{A.2}$$

where $E_{3i}^{(j)}$ and $H_{3i}^{(j)}$ are defined, in Eq. (33) and $\hat{E}_{3i}^{(j)}$ and $\hat{H}_{3i}^{(j)}$ are determined as

$$\left(\hat{E}_{3i}^{(j)}, \hat{H}_{3i}^{(j)}\right) = \int_{z_3}^{z_4} e_{3i}^{(j)}(1, z) f_j'(z) dz \tag{A.3}$$

and

$$\left(A_{ij}, B_{ij}, D_{ij}\right) = \sum_{k=1}^{3} \int_{z_k}^{z_{k+1}} Q_{ij}^{(k)}\left(1, z, z^2\right) dz \tag{A.4}$$

in which

$$Q_{11}^{(1),(3)}(z) = \frac{E_{11}^{(1),(3)}(z)}{1 - \nu_{12}^{(1),(3)}(z) \nu_{21}^{(1),(3)}(z)}, Q_{22}^{(1),(3)}(z) = \frac{E_{22}^{(1),(3)}(z)}{1 - \nu_{12}^{(1),(3)}(z) \nu_{21}^{(1),(3)}(z)},$$
$$Q_{12}^{(1),(3)}(z) = \frac{\nu_{12}^{(1),(3)}(z) E_{22}^{(1),(3)}(z)}{1 - \nu_{12}^{(1),(3)}(z) \nu_{21}^{(1),(3)}(z)}, Q_{66}^{(1),(3)}(z) = \frac{E_{11}^{(1),(3)}(z)}{2\left(1 + \nu_{12}^{(1),(3)}(z)\right)} \tag{A.5}$$
$$Q_{11}^{(2)}(z) = \frac{E_{11}^{(2)}(z)}{1 - \nu_{12}^{(2)}(z) \nu_{21}^{(2)}(z)}, Q_{22}^{(2)}(z) = \frac{E_{22}^{(2)}(z)}{1 - \nu_{12}^{(2)}(z) \nu_{21}^{(2)}(z)},$$

$$Q_{12}^{(2)}(z)=\frac{\nu_{12}^{(2)}(z)E_{22}^{(2)}(z)}{1-\nu_{12}^{(2)}(z)\nu_{21}^{(2)}(z)},Q_{66}^{(2)}(z)=\frac{E_{11}^{(2)}(z)}{2\left(1+\nu_{12}^{(2)}(z)\right)}$$

N_{xx}^{T} and N_{yy}^{T} are the thermal force resultants read as:

$$\begin{aligned}
&N_{xx}^{T}=\int_{z_1}^{z_2}\left(1+\nu^{(1)}\right)Q_{11}^{(1)}\alpha^{(1)}\Delta T dz+\int_{z_2}^{z_3}\left(1+\nu^{(2)}(z)\right)Q_{11}^{(2)}(z)\alpha^{(2)}(z)\Delta T dz\\
&+\int_{z_3}^{z_4}\left(1+\nu^{(3)}\right)Q_{11}^{(3)}\alpha^{(3)}\Delta T dz\\
&N_{yy}^{T}=\int_{z_1}^{z_2}\left(1+\nu^{(1)}\right)Q_{22}^{(1)}\alpha^{(1)}\Delta T dz+\int_{z_2}^{z_3}\left(1+\nu^{(2)}(z)\right)Q_{22}^{(2)}(z)\alpha^{(2)}(z)\Delta T dz\\
&+\int_{z_3}^{z_4}\left(1+\nu^{(3)}\right)Q_{22}^{(3)}\alpha^{(3)}\Delta T dz
\end{aligned} \tag{A.6}$$

The higher order moment resultants are as follow:

$$\begin{Bmatrix} Y_{xx}\\ Y_{yy}\\ Y_{xy}\\ Y_{xz}\\ Y_{yz}\end{Bmatrix}=\sum_{k=1}^{3}\int_{z_k}^{z_{k+1}}\begin{Bmatrix} m_{xx}^{(k)}\\ m_{yy}^{(k)}\\ m_{xy}^{(k)}\\ m_{xz}^{(k)}\\ m_{yz}^{(k)}\end{Bmatrix}dz \tag{A.7}$$

where they are reshuffled to:

$$\begin{aligned}
&Y_{xx}=C_1\left(\frac{\partial^2 w}{\partial x\,\partial y}\right),\ Y_{yy}=-C_1\left(\frac{\partial^2 w}{\partial x\,\partial y}\right),Y_{xy}=\frac{1}{2}C_1\left(\frac{\partial^2 w}{\partial y^2}-\frac{\partial^2 w}{\partial x^2}\right),\\
&Y_{yz}=\frac{1}{4}C_1\left(\frac{\partial^2 v_0}{\partial x\,\partial y}-\frac{\partial^2 u_0}{\partial y^2}\right),Y_{xz}=\frac{1}{4}C_1\left(\frac{\partial^2 v_0}{\partial x^2}-\frac{\partial^2 u_0}{\partial x\,\partial y}\right)
\end{aligned} \tag{A.8}$$

in which

$$C_1=2\sum_{k=1}^{3}\int_{z_k}^{z_{k+1}}\mu_k(z)l_k{}^2dz \tag{A.9}$$

The final nonlinear governing partial differential equations of the micro plate:

$$
\begin{aligned}
&B_{11}\left(\frac{\partial^3 u_0}{\partial x^3}+\left(\frac{\partial^2 w}{\partial x^2}\right)^2+\left(\frac{\partial w}{\partial x}\right)\left(\frac{\partial^3 w}{\partial x^3}\right)\right)+B_{12}\left(\frac{\partial^3 v_0}{\partial y\,\partial x^2}+\left(\frac{\partial^2 w}{\partial y\,\partial x}\right)^2+\left(\frac{\partial w}{\partial y}\right)\left(\frac{\partial^3 w}{\partial y\,\partial x^2}\right)\right)\\
&-D_{11}\left(\frac{\partial^4 w}{\partial x^4}\right)-2D_{12}\left(\frac{\partial^4 w}{\partial x^2\partial y^2}\right)+H_{31}^{(3)}\left(\frac{\partial^2 \psi_3}{\partial x^2}\right)+H_{31}^{(1)}\left(\frac{\partial^2 \psi_1}{\partial x^2}\right)\\
&+B_{12}\left(\frac{\partial^3 u_0}{\partial x\,\partial y^2}+\left(\frac{\partial^2 w}{\partial y\,\partial x}\right)^2+\left(\frac{\partial w}{\partial x}\right)\left(\frac{\partial^3 w}{\partial x\,\partial y^2}\right)\right)+B_{22}\left(\frac{\partial^3 v_0}{\partial y^3}+\left(\frac{\partial^2 w}{\partial y^2}\right)^2+\left(\frac{\partial w}{\partial y}\right)\left(\frac{\partial^3 w}{\partial y^3}\right)\right)+\\
&2B_{66}\left(\frac{\partial^3 u_0}{\partial x\,\partial y^2}+\frac{\partial^3 v_0}{\partial y\,\partial x^2}+\left(\frac{\partial w}{\partial y}\right)\left(\frac{\partial^3 w}{\partial y\,\partial x^2}\right)+\left(\frac{\partial^2 w}{\partial x^2}\right)\left(\frac{\partial^2 w}{\partial y^2}\right)+\left(\frac{\partial^2 w}{\partial y\,\partial x}\right)^2+\left(\frac{\partial w}{\partial x}\right)\left(\frac{\partial^3 w}{\partial x\,\partial y^2}\right)\right)\\
&-D_{22}\left(\frac{\partial^4 w}{\partial y^4}\right)+H_{32}^{(3)}\left(\frac{\partial^2 \psi_3}{\partial y^2}\right)+H_{32}^{(1)}\left(\frac{\partial^2 \psi_1}{\partial y^2}\right)-4D_{66}\left(\frac{\partial^4 w}{\partial x^2\partial y^2}\right)+C_1\left(\frac{1}{2}\frac{\partial^4 w}{\partial x^2\partial y^2}-\frac{1}{2}\frac{\partial^4 w}{\partial x^4}\right)\\
&-C_1\left(\frac{1}{2}\frac{\partial^4 w}{\partial y^4}-\frac{1}{2}\frac{\partial^4 w}{\partial x^2\partial y^2}\right)-2C_1\left(\frac{\partial^4 w}{\partial x^2\partial y^2}\right)-I_0\left(\frac{\partial^2 w}{\partial t^2}\right)+I_2\left(\frac{\partial^4 w}{\partial y^2\partial t^2}+\frac{\partial^4 w}{\partial x^2\partial t^2}\right)\\
&-I_1\left(\frac{\partial^3 u_0}{\partial x\,\partial t^2}+\frac{\partial^3 v_0}{\partial y\,\partial t^2}\right)+A_{11}\left(\frac{\partial u_0}{\partial x}+\frac{1}{2}\left(\frac{\partial w}{\partial x}\right)^2\right)\left(\frac{\partial^2 w}{\partial x^2}\right)+A_{12}\left(\frac{\partial v_0}{\partial y}+\frac{1}{2}\left(\frac{\partial w}{\partial y}\right)^2\right)\left(\frac{\partial^2 w}{\partial x^2}\right)\\
&+\left(-B_{11}\left(\frac{\partial^2 w}{\partial x^2}\right)-B_{12}\left(\frac{\partial^2 w}{\partial y^2}\right)+E_{31}^{(1)}\psi_1+E_{31}^{(3)}\psi_3+\hat{H}_{31}^{(1)}V\left(t\right)+\hat{H}_{31}^{(3)}V\left(t\right)+N_{xx}^{T}\right)\left(\frac{\partial^2 w}{\partial x^2}\right)\\
&+A_{12}\left(\frac{\partial u_0}{\partial x}+\frac{1}{2}\left(\frac{\partial w}{\partial x}\right)^2\right)\left(\frac{\partial^2 w}{\partial y^2}\right)+A_{22}\left(\frac{\partial v_0}{\partial y}+\frac{1}{2}\left(\frac{\partial w}{\partial y}\right)^2\right)\left(\frac{\partial^2 w}{\partial y^2}\right)\\
&+\left(-B_{12}\left(\frac{\partial^2 w}{\partial x^2}\right)-B_{22}\left(\frac{\partial^2 w}{\partial y^2}\right)+E_{32}^{(1)}\psi_1+E_{32}^{(3)}\psi_3+\hat{H}_{32}^{(1)}V\left(t\right)+\hat{H}_{32}^{(3)}V\left(t\right)+N_{yy}^{T}\right)\left(\frac{\partial^2 w}{\partial y^2}\right)+\\
&\left(2A_{66}\left(\frac{\partial u_0}{\partial y}+\frac{\partial v_0}{\partial x}+\left(\frac{\partial w}{\partial x}\right)\left(\frac{\partial w}{\partial y}\right)\right)-4B_{66}\left(\frac{\partial^2 w}{\partial y\,\partial x}\right)\right)\left(\frac{\partial^2 w}{\partial y\,\partial x}\right)-P_{xx}\left(\frac{\partial^2 w}{\partial x^2}\right)-P_{yy}\left(\frac{\partial^2 w}{\partial y^2}\right)=0
\end{aligned}
\tag{A.10}
$$

$$
\begin{aligned}
&A_{11}\left(\frac{\partial^2 u_0}{\partial x^2}+\left(\frac{\partial w}{\partial x}\right)\left(\frac{\partial^2 w}{\partial x^2}\right)\right)-\frac{1}{8}C_1\left(\frac{\partial^4 u_0}{\partial y^4}\right)+A_{12}\left(\frac{\partial^2 v_0}{\partial y\,\partial x}+\left(\frac{\partial w}{\partial y}\right)\left(\frac{\partial^2 w}{\partial y\,\partial x}\right)\right)-\frac{1}{8}C_1\left(\frac{\partial^4 u_0}{\partial x^2\partial y^2}\right)\\
&-B_{11}\left(\frac{\partial^3 w}{\partial x^3}\right)-B_{12}\left(\frac{\partial^3 w}{\partial x\,\partial y^2}\right)+E_{31}^{(1)}\left(\frac{\partial \psi_1}{\partial x}\right)+E_{31}^{(3)}\left(\frac{\partial \psi_3}{\partial x}\right)+A_{66}\left(\frac{\partial^2 u_0}{\partial y^2}\right)+A_{66}\left(\frac{\partial^2 v_0}{\partial y\,\partial x}\right)\\
&+A_{66}\left(\left(\frac{\partial w}{\partial y}\right)\left(\frac{\partial^2 w}{\partial y\,\partial x}\right)+\left(\frac{\partial w}{\partial x}\right)\left(\frac{\partial^2 w}{\partial y^2}\right)\right)+I_1\left(\frac{\partial^3 w}{\partial x\,\partial t^2}\right)+\frac{1}{8}C_1\left(\frac{\partial^4 v_0}{\partial x^3\partial y}\right)-2B_{66}\left(\frac{\partial^3 w}{\partial x\,\partial y^2}\right)\\
&+\frac{1}{8}C_1\left(\frac{\partial^4 v_0}{\partial y^3\partial x}\right)-I_0\left(\frac{\partial^2 u_0}{\partial t^2}\right)=0
\end{aligned}
\tag{A.11}
$$

$$A_{22}\left(\frac{\partial^2 v_0}{\partial y^2}+\left(\frac{\partial w}{\partial y}\right)\left(\frac{\partial^2 w}{\partial y^2}\right)\right)-\frac{1}{8}C_1\left(\frac{\partial^4 v_0}{\partial x^4}\right)+A_{12}\left(\frac{\partial^2 u_0}{\partial y\,\partial x}+\left(\frac{\partial w}{\partial x}\right)\left(\frac{\partial^2 w}{\partial y\,\partial x}\right)\right)-\frac{1}{8}C_1\left(\frac{\partial^4 v_0}{\partial x^2\partial y^2}\right)$$
$$-B_{22}\left(\frac{\partial^3 w}{\partial y^3}\right)-B_{12}\left(\frac{\partial^3 w}{\partial y\,\partial x^2}\right)+E_{32}^{(1)}\left(\frac{\partial \psi_1}{\partial y}\right)+E_{32}^{(3)}\left(\frac{\partial \psi_3}{\partial y}\right)+A_{66}\left(\frac{\partial^2 u_0}{\partial x^2}\right)+A_{66}\left(\frac{\partial^2 u_0}{\partial y\,\partial x}\right)$$
$$+A_{66}\left(\left(\frac{\partial w}{\partial x}\right)\left(\frac{\partial^2 w}{\partial y\,\partial x}\right)+\left(\frac{\partial w}{\partial y}\right)\left(\frac{\partial^2 w}{\partial x^2}\right)\right)+I_1\left(\frac{\partial^3 w}{\partial y\,\partial t^2}\right)+\frac{1}{8}C_1\left(\frac{\partial^4 u_0}{\partial x^3\partial y}\right)-2B_{66}\left(\frac{\partial^3 w}{\partial y\,\partial x^2}\right) \quad \text{(A.12)}$$
$$+\frac{1}{8}C_1\left(\frac{\partial^4 u_0}{\partial y^3\partial x}\right)-I_0\left(\frac{\partial^2 v_0}{\partial t^2}\right)=0$$

$$\int_{z_3}^{z_4}\left(-\phi_3^{\,2}\left(k_{11}^{(3)}\frac{\partial^2 \psi_3}{\partial x^2}+k_{22}^{(3)}\frac{\partial^2 \psi_3}{\partial y^2}\right)+k_{33}^{(3)}\phi_{3,z}\left(\phi_{3,z}\psi_3+Vf_3'(z)\right)-p_3^{(3)}\phi_{3,z}\Delta T\right)dz$$
$$-\frac{1}{2}\left(E_{31}^{(3)}\left(\frac{\partial w}{\partial x}\right)^2+E_{32}^{(3)}\left(\frac{\partial w}{\partial y}\right)^2\right)-\left(E_{31}^{(3)}\frac{\partial u_0}{\partial x}+E_{32}^{(3)}\frac{\partial v_0}{\partial y}\right)+\left(H_{31}^{(3)}\frac{\partial^2 w}{\partial x^2}+H_{32}^{(3)}\frac{\partial^2 w}{\partial y^2}\right)=0 \quad \text{(A.13)}$$

$$\int_{z_1}^{z_2}\left(-\phi_1^{\,2}\left(k_{11}^{(1)}\frac{\partial^2 \psi_1}{\partial x^2}+k_{22}^{(1)}\frac{\partial^2 \psi_1}{\partial y^2}\right)+k_{33}^{(1)}\phi_{1,z}\left(\phi_{1,z}\psi_1+Vf_1'(z)\right)-p_3^{(1)}\phi_{1,z}\Delta T\right)dz$$
$$-\frac{1}{2}\left(E_{31}^{(1)}\left(\frac{\partial w}{\partial x}\right)^2+E_{32}^{(1)}\left(\frac{\partial w}{\partial y}\right)^2\right)-\left(E_{31}^{(1)}\frac{\partial u_0}{\partial x}+E_{32}^{(1)}\frac{\partial v_0}{\partial y}\right)+\left(H_{31}^{(1)}\frac{\partial^2 w}{\partial x^2}+H_{32}^{(1)}\frac{\partial^2 w}{\partial y^2}\right)=0 \quad \text{(A.14)}$$

The boundary conditions at $x=0,a$:

$$\frac{\partial M_{xx}}{\partial x}+\frac{\partial M_{xy}}{\partial y}+N_{xx}\frac{\partial w}{\partial x}+N_{xy}\frac{\partial w}{\partial y}+\frac{\partial Y_{xy}}{\partial x}-\frac{1}{2}\frac{\partial Y_{xx}}{\partial y}+\frac{1}{2}\frac{\partial Y_{yy}}{\partial y}-I_2\frac{\partial \ddot{w}}{\partial x}+I_1\ddot{u}_0=0 \text{ or } \delta w=0 \quad \text{(A.15)}$$

$$-N_{xx}-\frac{1}{4}\frac{\partial Y_{xz}}{\partial y}\Bigg|x=0,a=0 \text{ or } \delta u_0=0 \quad \text{(A.16)}$$

$$-N_{xy}+\frac{1}{4}\frac{\partial Y_{yz}}{\partial y}+\frac{1}{2}\frac{\partial Y_{xz}}{\partial x}\Bigg|x=0,a=0 \text{ or } \delta v_0=0 \quad \text{(A.17)}$$

$$\int_{z_3}^{z_4}\left(-k_{11}^{(3)}\phi_3^{\,2}\left(\frac{\partial \psi_3}{\partial x}\right)+p_1^{(3)}\phi_3\Delta T\right)dz\Bigg|x=0,a=0 \text{ or } \delta\psi_3=0 \quad \text{(A.18)}$$

$$\int_{z_1}^{z_2}\left(-k_{11}^{(1)}\phi_1^{\,2}\left(\frac{\partial \psi_1}{\partial x}\right)+p_1^{(1)}\phi_1\Delta T\right)dz\Bigg|x=0,a=0 \text{ or } \delta\psi_1=0 \quad \text{(A.19)}$$

$$M_{xx}+Y_{xy}\Bigg|x=0,a=0 \text{ or } \delta\frac{\partial w}{\partial x}=0 \quad \text{(A.20)}$$

$$M_{xy}-\frac{1}{2}Y_{xx}+\frac{1}{2}Y_{yy}\Bigg|x=0,a=0 \text{ or } \delta\frac{\partial w}{\partial y}=0 \quad \text{(A.21)}$$

$$Y_{xz}\Big|x=0,a=0 \text{ or } \delta\frac{\partial u_0}{\partial y}=0 \quad \text{(A.22)}$$

$$Y_{yz}\Big|_{x=0,a}=0 \text{ or } \delta\frac{\partial v_0}{\partial y}=0 \tag{A.23}$$

$$Y_{xz}\Big|_{x=0,a}=0 \text{ or } \delta\frac{\partial v_0}{\partial x}=0 \tag{A.24}$$

The boundary conditions at $y=0,b$:

$$\frac{\partial M_{yy}}{\partial y}+\frac{\partial M_{xy}}{\partial x}+N_{yy}\frac{\partial w}{\partial y}+N_{xy}\frac{\partial w}{\partial x}-\frac{\partial Y_{xy}}{\partial y}-\frac{1}{2}\frac{\partial Y_{xx}}{\partial x}+\frac{1}{2}\frac{\partial Y_{yy}}{\partial x}-I_2\frac{\partial \ddot{w}}{\partial y}+I_1\ddot{v}_0\Big|_{y=0,b}=0 \text{ or } \delta w=0 \tag{A.25}$$

$$-N_{xy}+\frac{1}{4}\frac{\partial Y_{xz}}{\partial x}-\frac{1}{2}\frac{\partial Y_{yz}}{\partial y}\Big|_{y=0,b}=0 \text{ or } \delta u_0=0 \tag{A.26}$$

$$-N_{yy}-\frac{1}{4}\frac{\partial Y_{yz}}{\partial x}\Big|_{y=0,b}=0 \text{ or } \delta v_0=0 \tag{A.27}$$

$$\int_{z_3}^{z_4}\left(-k_{22}^{(3)}\phi_3{}^2\left(\frac{\partial \psi_3}{\partial y}\right)+p_2^{(3)}\phi_3\Delta T\right)dz\Big|_{y=0,b}=0 \text{ or } \delta\psi_3=0 \tag{A.28}$$

$$\int_{z_1}^{z_2}\left(-k_{22}^{(1)}\phi_1{}^2\left(\frac{\partial \psi_1}{\partial y}\right)+p_2^{(1)}\phi_1\Delta T\right)dz\Big|_{y=0,b}=0 \text{ or } \delta\psi_1=0 \tag{A.29}$$

$$M_{yy}-Y_{xy}\Big|_{y=0,b}=0 \text{ or } \delta\frac{\partial w}{\partial y}=0 \tag{A.30}$$

$$M_{xy}-\frac{1}{2}Y_{xx}+\frac{1}{2}Y_{yy}\Big|_{y=0,b}=0 \text{ or } \delta\frac{\partial w}{\partial x}=0 \tag{A.31}$$

$$Y_{xz}\Big|_{y=0,b}=0 \text{ or } \delta\frac{\partial u_0}{\partial x}=0 \tag{A.32}$$

$$Y_{yz}\Big|_{y=0,b}=0 \text{ or } \delta\frac{\partial u_0}{\partial y}=0 \tag{A.33}$$

$$Y_{yz}\Big|_{y=0,b}=0 \text{ or } \delta\frac{\partial v_0}{\partial x}=0 \tag{A.34}$$

REFERENCES

[1] M.A. Farsangi, A. Saidi, R. Batra, Analytical solution for free vibrations of moderately thick hybrid piezoelectric laminated plates, Journal of Sound and Vibration, 332(22) (2013) 5981-5998.

[2] Y. Kiani, Free vibration of functionally graded carbon nanotube reinforced composite plates integrated with piezoelectric layers, Computers & Mathematics with Applications, 72(9) (2016) 2433-2449.

[3] M. Bouazza, A.M. Zenkour, Vibration of carbon nanotube-reinforced plates via refined nth-higher-order theory, ARCHIVE OF APPLIED MECHANICS, (2020) https://doi.org/10.1007/s00419-020-01694-3.

[4] H.-S. Shen, Y. Xiang, F. Lin, Nonlinear vibration of functionally graded graphene-reinforced composite laminated plates in thermal environments, Computer Methods in Applied Mechanics and Engineering, 319 (2017) 175-193.

[5] M. Song, S. Kitipornchai, J. Yang, Free and forced vibrations of functionally graded polymer composite plates reinforced with graphene nanoplatelets, Composite Structures, 159 (2017) 579-588.

[6] E. Garcia-Macias, L. Rodriguez-Tembleque, A. Saez,

Bending and free vibration analysis of functionally graded graphene vs. carbon nanotube reinforced composite plates, Composite Structures, 186 (2018) 123-138.

[7] R. Gholami, R. Ansari, Nonlinear harmonically excited vibration of third-order shear deformable functionally graded graphene platelet-reinforced composite rectangular plates, Engineering Structures, 156 (2018) 197-209.

[8] S. Qaderi, F. Ebrahimi, V. Mahesh, Free vibration analysis of graphene platelets–reinforced composites plates in thermal environment based on higher-order shear deformation plate theory, International Journal of Aeronautical and Space Sciences, 20(4) (2019) 902-912.

[9] F. Pashmforoush, Statistical analysis on free vibration behavior of functionally graded nanocomposite plates reinforced by graphene platelets, Composite Structures, 213 (2019) 14-24.

[10] A.R. Saidi, R. Bahaadini, K. Majidi-Mozafari, On vibration and stability analysis of porous plates reinforced by graphene platelets under aerodynamical loading, Composites Part B: Engineering, 164 (2019) 778-799.

[11] 11. W. Chen, X. Li, A new modified couple stress theory for anisotropic elasticity and microscale laminated Kirchhoff plate model, Archive of Applied Mechanics, 84(3) (2014) 323-341.

[12] Y.-G. Wang, W.-H. Lin, C.-L. Zhou, Nonlinear bending of size-dependent circular microplates based on the modified couple stress theory, Archive of Applied Mechanics, 84(3) (2014) 391-400.

[13] Y. Yue, K. Xu, Z. Tan, W. Wang, D. Wang, The influence of surface stress and surface-induced internal residual stresses on the size-dependent behaviors of Kirchhoff microplate, Archive of Applied Mechanics, 89(7) (2019) 1301-1315.

[14] S.-R. Li, H.-K. Ma, Analysis of free vibration of functionally graded material micro-plates with thermoelastic damping, Archive of Applied Mechanics, 90 (2020) 1285–1304.

[15] F. Abbaspour, H. Arvin, Vibration and thermal buckling analyses of three-layered centrosymmetric piezoelectric microplates based on the modified consistent couple stress theory, Journal of Vibration and Control, 26(15-16) (2020) 1253-1265.

[16] M. Arefi, M. Kiani, A.M. Zenkour, Size-dependent free vibration analysis of a three-layered exponentially graded nano-/micro-plate with piezomagnetic face sheets resting on Pasternak's foundation via MCST, Journal of Sandwich Structures & Materials, 22(1) (2020) 55-86.

[17] H. Arvin, The flapwise bending free vibration analysis of micro-rotating Timoshenko beams using the differential transform method, Journal of Vibration and Control, 24(20) (2018) 4868-4884.

[18] J.N. Reddy, Mechanics of laminated composite plates and shells: theory and analysis, CRC press, 2003.

[19] Q. Wang, On buckling of column structures with a pair of piezoelectric layers, Engineering structures, 24(2) (2002) 199-205.

[20] H. Wu, S. Kitipornchai, J. Yang, Thermal buckling and postbuckling of functionally graded graphene nanocomposite plates, Materials & Design, 132 (2017) 430-441.

[21] Y. Huang, Z. Yang, A. Liu, J. Fu, Nonlinear buckling analysis of functionally graded graphene reinforced composite shallow arches with elastic rotational constraints under uniform radial load, Materials, 11(6) (2018) 910.

[22] L. Meirovitch, Principles and techniques of vibrations, Prentice Hall Upper Saddle River, NJ, 1997.

[23] N.V. Nguyen, J. Lee, H. Nguyen-Xuan, Active vibration control of GPLs-reinforced FG metal foam plates with piezoelectric sensor and actuator layers, Composites Part B: Engineering, 172 (2019) 769-784.

[24] E. Jomehzadeh, H. Noori, A. Saidi, The size-dependent vibration analysis of micro-plates based on a modified couple stress theory, Physica E: Low-dimensional Systems and Nanostructures, 43(4) (2011) 877-883.

[25] M. Shariyat, Dynamic buckling of imperfect laminated plates with piezoelectric sensors and actuators subjected to thermo-electro-mechanical loadings, considering the temperature-dependency of the material properties, Composite Structures, 88(2) (2009) 228-239.

HOW TO CITE THIS ARTICLE

F. Abbaspour, H. Arvin, Vibration analysis of piezoelectric graphene platelets micro-plates, AUT J. Mech Eng., 5(3) (2021) 361-386.

DOI: 10.22060/ajme.2021.18655.5911